JOURNAL OF GEOPHYSICAL RESEARCH, VOL. 103, NO. B8, PAGES 17,749–17,766, AUGUST 10, 1998

Modeling Cenozoic sedimentation in the central equatorial Pacific and implications for true polar wander

Neil C. Mitchell

Department of Earth Sciences, University of Oxford, Oxford, England
and Department of Geological Sciences, University of Durham, Durham, England

Abstract. High productivity along the central Pacific equator has left thick deposits of calcareous and siliceous ooze. West of 102°W, these have deposited on the Pacific plate which has been drifting northwards and therefore the thickest deposits are displaced north of the equator. This study attempts to simulate the sediment distribution using information from Deep Sea Drilling Project (DSDP) cores and models for Pacific plate motion. The DSDP core data are used to account for accumulation rate variations with time, paleolatitude and paleodepth, accounting for variable carbonate dissolution. The model predicts the distribution on 35-50 Ma seafloor relatively well and demonstrates that the sedimentary bulge is distorted by variable dissolution over a regional bathymetry gradient due to the northern edge of the South Pacific Superswell. A westerly deepening of the carbonate compensation depth and sedimentary lysocline evolution are proposed, which improve the model for seafloor 30 Ma and older. The degree of match between model and data provides a test of the amount of northward drift of the Pacific plate and, assuming a model for Pacific hotspots motion, of true polar wander (TPW, motion of the hotspot frame relative to the Earth's spin axis). Assuming the *Duncan and Clague* [1985] model for Pacific hotspots motion, the sedimentary modeling favors TPW models which have little or no effect on the central Pacific paleoequator over the past 30 Ma. We also explore implications of interhotspot motion and the suggestion that the bend in the Hawaiian volcanic chain represents an abrupt change in Pacific hotspot motion within the last 5 Ma.

1. Introduction

Upwelling of nutrient rich deep waters along the equator of the modern Pacific Ocean, and their mixing with warm tropical waters by the equatorial current system, lead to high productivity of pelagic organisms in surface waters [e.g., *Arrhenius*, 1952]. Accumulation of these organisms' tests during the Cenozoic has left thick deposits of calcareous and siliceous ooze (Figure 1a). These sediments have received much attention from the Deep Sea Drilling Project (DSDP) and Ocean Drilling Program (ODP) because they record information on ancient water circulation and properties, they form an important component of the ocean carbon cycle and, assuming sedimentation has remained centered on the equator, record motions of the Pacific tectonic plate. Syntheses of DSDP cores for the later Cenozoic [*Berger*, 1973, 1978; *Berger and Winterer*, 1974; *Lancelot*, 1978; *Leinen*, 1979; *van Andel et al.*, 1975; *Worsley and Davies*, 1979] reveal an east-west zone of enhanced pelagic sedimentation, modified by varying carbonate dissolution with depth and by bottom-current erosion which has left hiatuses in many areas, mostly north of the equatorial zone. Some variation in sediment composition and productivity occurs along the zone [e.g., *Theyer et al.*, 1985], as revealed in particular by silica accumulation rates [*Leinen*, 1979], which are less complicated by variable dissolution with depth, but this longitudinal variation is much weaker than the latitudinal variation. The sediments supplied along the equator have accumulated on the Pacific plate which is itself drifting northwards relative to the equator. This has produced the stratigraphy illustrated in Figure 2, in which, as a result of the northward plate drift, the bulge lies generally north of the equator and is broader than might be expected from the latitude extent of present-day sedimentation.

This study attempts to model the overall distribution of Cenozoic sediments represented by a newly released sediment thickness database (Figure 1a), using accumulation rate data from DSDP cores, an approach originally attempted by *Winterer* [1973] and *Clague and Jarrard* [1973]. The purpose is twofold: first, to test the conceptual model of equatorial sedimentation derived from the DSDP cores [*van Andel et al.*, 1975] and, second, to test kinematic models for the Pacific plate. Of the former, the modeling largely confirms the conceptual model though highlights some anomalies that require explanation. For example, the conceptual model can be improved by considering that reduced dissolution occurs west of 135° W, which can be modeled by a regional variation of the carbonate compensation depth (CCD) similar to that observed in the present day CCD.

True polar wander (TPW), as considered here, is the slow motion of the hotspot reference frame, assumed to represent the lower mantle, relative to the Earth's spin axis caused by the evolving distribution of mass in the Earth such as due to descending lithospheric slabs and mantle convection [e.g., *Goldreich and Toomre*, 1969]. TPW is expected to lag behind the polar wander predicted from changes in the solid (nonrotating) Earth mass distribution because of the stabilizing effect of the Earth's hydrostatic bulge, so modeling this dampened motion can potentially help to constrain mantle viscosity structure [e.g., *Richards et al.*, 1997; *Steinberger and O'Connell*, 1997]. TPW can be most accurately modeled during the late Cenozoic because slab evolution from plate geometries and motions is best constrained during this interval. The amount of TPW during 0-50

Paper number 98JB01577
0148-0227/98/98JB-01577$09.00

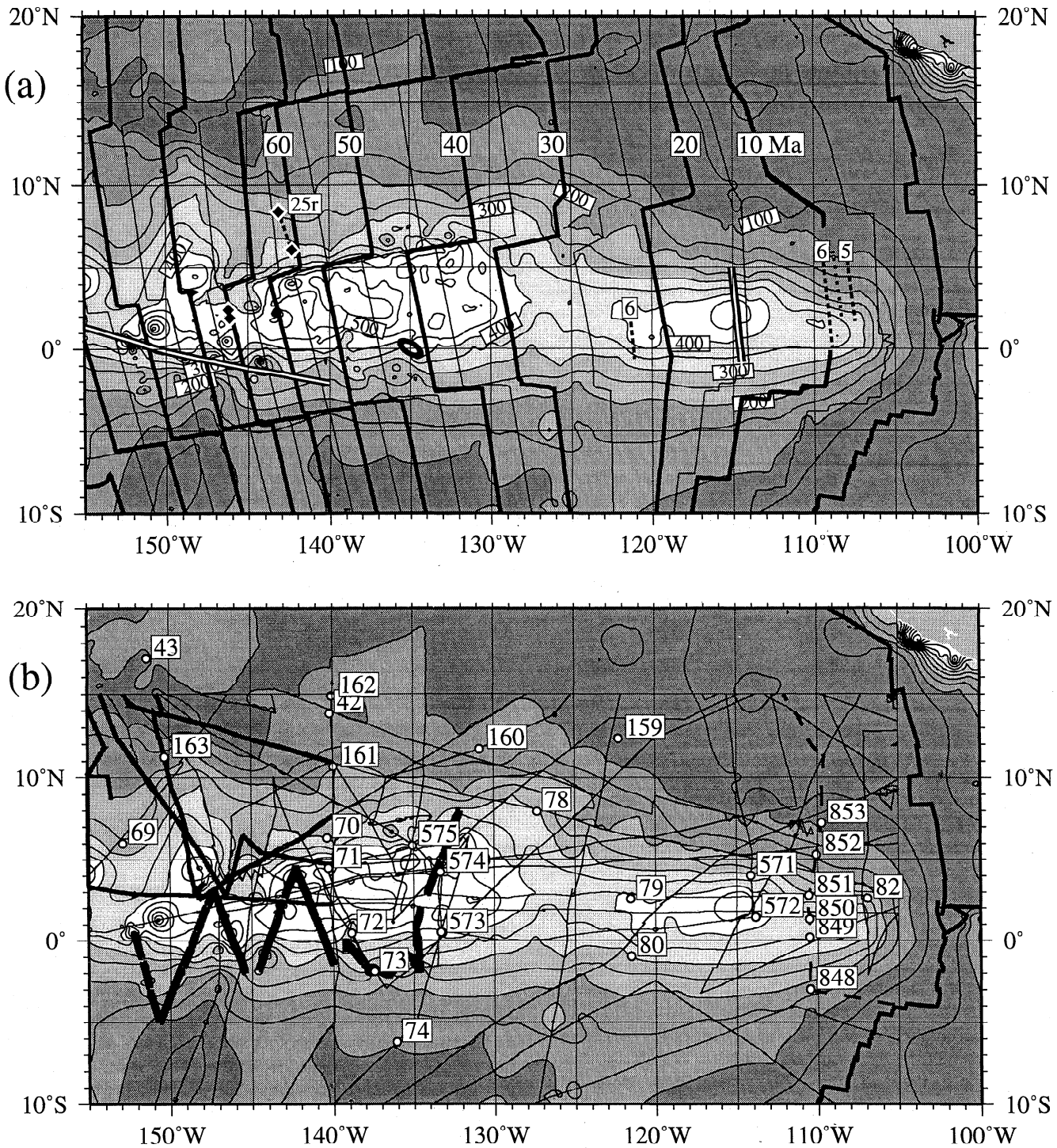

Figure 1. (a) Sediment thickness in the equatorial Pacific Ocean from an NGDC database [*Divins and Eakins*, 1997] is shown contoured every 50 m. The overlain lines are 5 m.y. isochrons from a seafloor age database [*Muller et al.*, 1997]. The double ruled line running across the westerly isochrons locates a prominent "crossgrain" chain of volcanic ridges identified by *Winterer and Sandwell* [1987]. These ridges and a large elongate seamount (ellipse at 0°N, 135°W) are prominent features of the marine gravity field [*Sandwell and Smith*, 1997]. The double ruled line at 115°W and numbered dashed lines are the extinct ridge and associated anomalies 5 and 6 identified by *Herron* [1972]. The four solid diamond symbols in the west area are identifications of anomaly 25r of ~57 Ma age [*Petronotis et al.*, 1994]. (b) Distribution of seismic lines used to produce the sediment thickness map, mostly cruises of Lamont-Doherty Geological Observatory and Scripps Institution of Oceanography. Data from the bold dashed line at 110°W were used for Figure A1 (Venture 1 cruise of the R/V *Thomas Washington*). Numbers refer to DSDP and ODP drill sites. Medium bold highlights seismic data used by *Houtz and Ludwig* [1979] to map deep reverberant sediment layers (probably Eocene and older sediments containing chert layers). Heavy bold lines locate sections of seismic data from R/V *Thomas Washington* Crossgrain-1 cruise [*Winterer and Sandwell*, 1987] which were used to supplement the NGDC sediment thickness map.

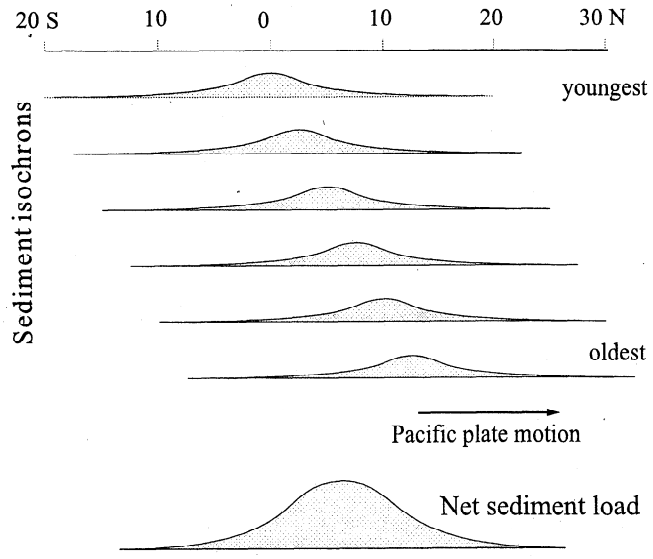

Figure 2. Schematic illustration of the effect of northward Pacific plate motion on sediment stratigraphy, adapted from *Berger and Winterer* [1974]. The sediment isochrons represent sedimentation intervals displaced to the north by varying amounts depending on sediment age and history of plate motion. The bottom graph represents the sediment load obtained by integrating the intervals. The net load is broader than individual isochrons and is offset from the equator by roughly half the total plate drift.

Ma is controversial, however, with some authors arguing for 8°-10° of motion [e.g., *Andrews*, 1985; *Besse and Courtillot*, 1991] and others arguing for less than 5° [e.g., *Livermore et al.*, 1983; *Sager and Pringle*, 1988]. The shape of the TPW path also varies between different studies. Furthermore, uncertainties concerning motions between hotspots has led some authors to question the extent to which the hotspot reference frame itself is a viable concept [e.g., *Christensen*, 1998]. The following modeling addresses the motion of the Pacific hotspots relative to the equator, and we discuss later the origin of disagreement between the different TPW paths.

The question of TPW is also important for palaeoceanographic studies because the form of sedimentation about the equator cannot be evaluated without independent paleolatitude information. Studies based on the ODP Leg 138 sediments, for example, have addressed latitude variations in the equatorial current system [*Pisias et al.*, 1995a] after sites were adjusted for plate motion using the *Cox and Engebretson* [1985] Pacific-hotspots poles. Some of the palaeoceanographic conclusions may be affected by unresolved Pacific-hotspots motion and polar wander that were not accounted for using the *Cox and Engebretson* [1985] poles.

The change in sign of the Coriolis effect deflects wind-driven surface currents to the right north of the equator and to the left south of the equator, causing divergence of surface waters. Upwelling of nutrient-rich deep waters balances this surface divergence and produces the high equatorial productivity. Assuming that the Coriolis effect has maintained high sedimentation centered on the equator, the equatorial sediment distribution may record the paleoequator on the Pacific plate. Since Pacific-hotspots motion is also relatively well known [e.g., *Duncan and Clague*, 1985], paleoequators may help to constrain TPW. Constraints provided by the sediments are independent of the paleomagnetic constraints, and several authors have interpreted paleoequators from enhanced accumulation rates and characteristic sedimentary facies in DSDP cores [*Berger*, 1973; *Clague and Jarrard*, 1973; *Gordon and Cape*, 1981; *Sager*, 1984; *Suarez and Molnar*, 1980; *van Andel et al.*, 1975; *Winterer*, 1973]. Although the most recent evaluations support a lack of TPW for the past 45 m.y. [*Gordon and Cape*, 1981; *Sager*, 1984; *Suarez and Molnar*, 1980], the interpretation of palcocquators in the limited number of cores available is complicated by possible local current and gravity redistribution and by variable dissolution and pelagic productivity with time. The modeling in this study, which incorporates variable carbonate dissolution and productivity, therefore seeks to confirm the prior results by effectively using the greater coverage provided by the seismic reflection records (Figure 1b) to overcome problems with the individual drill cores. The results generally support previous claims [*Gordon and Cape*, 1981; *Sager*, 1984; *Suarez and Molnar*, 1980] that the Pacific hotspots show little evidence for drift relative to the equator during the late Cenozoic.

2. Data Preparation and Assessment

2.1. Sediment Thicknesses

Figure 1a shows sediment thicknesses modified from a database released by the National Geophysical Data Center (NGDC) [*Divins and Eakins*, 1997]. The database was originally created by digitizing isopachs from *Ludwig and Houtz* [1979] and gridding with further seismic data available to the NGDC. We have upgraded the map using seismic data from the 1987 'Crossgrain-1' cruise of the R/V *Thomas Washington* [*Winterer and Sandwell*, 1987]. Seismic two-way time was digitized from the heavy bold lines in Figure 1b and converted to thickness with a velocity of 2 km/s as used by *Ludwig and Houtz* [1979]. The NGDC sediment thickness grid was sampled along the other lines shown in Figure 1b and regridded together with the Crossgrain-1 data using a tensioned surface fitting program [*Smith and Wessel*, 1990].

One potential limitation of the database is the extent to which interpreted acoustic basement corresponds to oceanic basement because highly reflective cherts of Eocene age occur west of ~130°W. The magnitude of this error is difficult to assess, although data from around the medium bold lines in Figure 1b may be less biased because these are profiles used by *Houtz and Ludwig* [1979] to map the thickness of the deep reflective layer. Due to this ambiguity, both total and post-Eocene accumulation were modeled for comparison with the sediment thickness data.

Intraplate volcanism is relatively uncommon in the central equatorial Pacific so sediments above volcanic basement can be assumed for the most part to have accumulated on oceanic crust created at the East Pacific Rise (EPR). The nearest seamount chain is the Marquesas lying south of 7°S, 145°W. However, *Winterer and Sandwell* [1987] described a chain of volcanic ridges (the double line on the west side of Figure 1a) that are significantly younger than oceanic basement and cut across normal oceanic trends. Volcanism associated with these ridges may locally mask older sedimentary units in the seismic records. The newly released gravity images [*Sandwell and Smith*, 1997] show that this chain of ridges is the most dominant such feature in this region, and we expect that the biasing effect of younger volcanism is probably confined to it. The ellipse in Figure 1a locates a major volcanic ridge, but the *Thomas Washington* seismic data suggest that it is an old feature.

The NGDC database was checked by comparing thicknesses with basement depths in DSDP and ODP cores. Including seven sites that the site reports suggest terminated just above basement,

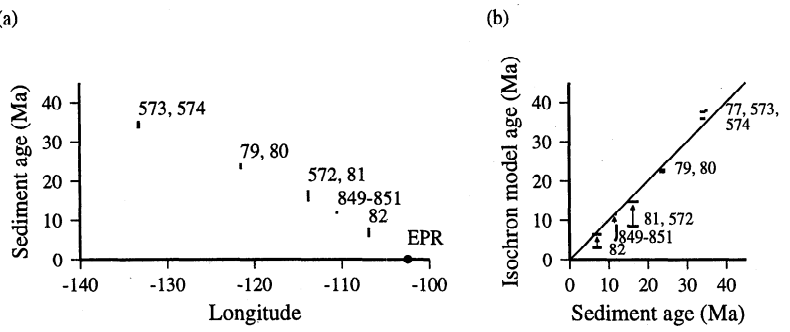

Figure 3. (a) Basal sediment ages at DSDP and ODP sites along the equator versus longitude. The age shown is (for Sites 79, 80, 81, and 82) the foraminifera zone range from *van Andel and Bukry* [1973] and (for Sites 572, 573, and 574) ages derived from *Barron et al.* [1985], all converted to the *Cande and Kent* [1995] timescale. ODP Sites 849-851 are given an age of 11.6-12.0 Ma from oldest sediment cored above basalt [*Shackleton et al.*, 1995]. EPR represents the East Pacific Rise. Note the higher apparent spreading rate east of 120°W, which has been attributed to ridge jumps incorporating elements of Cocos plate in Pacific seafloor [*Herron*, 1972; *van Andel et al.*, 1975; *Winterer*, 1976]. (b) Basal sediment ages compared to isochron model ages [*Muller et al.*, 1997] at the drill sites shown. Arrows show effect of adjusting 5, 10, and 15 Ma isochrons to the configuration shown in Figure 1a.

the mean difference for 24 sites is 10 m with 50 m standard deviation. There are some large discrepancies between individual sites and the database, but these can mostly be explained by local redistribution seen in site survey data, except for a discrepancy of 100 m for Site 80 (199 m deep) which is anomalous. Furthermore, the database may still have some bias owing to seismic velocity error and, considering also the incomplete coverage, the modeling here addresses only broad trends in the sediment thickness map.

2.2. Isochron Model

In order to study the sedimentation as a function of seafloor age, we have adopted the seafloor isochron model in Figure 1a, which is based on that of *Muller et al.* [1997]. The impact of errors in the isochron map on the sedimentation modeling depends on whether seafloor is older or younger than the Eocene-Oligocene boundary, because post-Eocene accumulation rates were much higher than those of Eocene age or earlier and because the sediment thickness map may represent mostly post-Eocene sediments due to the reverberant Eocene cherts mentioned earlier. Therefore, west of 125°, mismatches between fracture zones in these isochrons and those observed in gravity anomaly maps [*Sandwell and Smith*, 1997], generally less than 100 km within 10° of the equator, and small mismatches between isochrons compared to some recent identifications (e.g., of 2°-3° of longitude [*Eittreim et al.*, 1992]), have little effect on the following study. The same applies to a more significant bias in the west of the isochron map highlighted by *Petronotis et al.*'s [1994] location of anomaly 25r (57 Ma). Their two identifications south of the Clipperton fracture zone (4°N, 146°W) lie significantly west of the corresponding isochrons in the model by ~400 km, but the 13 m.y. age error still has little effect in the modeling. Effects of these age errors are illustrated more quantitatively later.

Seafloor east of 125°W is more problematic, however. Figure 3a shows sediment age at the base of DSDP cores versus longitude and reveals a steeper slope east of 120°W (~1.4 m.y./°longitude) than west of 120°W (~0.9 m.y./°). This rapid rate of age progression is also ~30% higher than that calculated from seafloor spreading anomalies outside the equatorial zone, suggesting that ridge jumps or other mechanisms have incorporated sections of Cocos seafloor in the Pacific plate [*Herron*, 1972; *van Andel et al.*, 1975; *Winterer*, 1976]. *Herron*'s [1972] proposed extinct ridge and anomaly 5 and 6 identifications are shown in Figure 1a (double line at 115°W and dashed lines, respectively) and illustrate the ambiguity in these younger isochrons. The spreading pattern implied by *Herron*'s [1972] identifications is inconsistent with the sediment thicknesses, which increase toward the fossil ridge at 125°W rather than decreasing from anomaly 6 seafloor on either side, a fault that could lie with either the sediment thickness map or the anomaly identifications. Furthermore, ODP Sites 849-851 just west of 110°W should lie on seafloor slightly younger than chron 6 (19-20 Ma) according to *Herron* [1972], but the site reports show no evidence for sediment older than 12 Ma [*Shackleton et al.*, 1995]. Until a better analysis of the magnetic anomalies can be carried out, we can only assume that seafloor generally increases to the west as constrained by the drill site basal sediment ages but that abrupt variations in basement age may occur between drill sites. We suspect, however, that these age errors are not much greater than 5 m.y. because of the spacing of drill core dates in Figure 3a. Furthermore, there are no microplates observable in the gravity field of the central equatorial Pacific [*Sandwell and Smith*, 1997]. This does not rule out the possibility of ~5 m.y. jumps in basement age associated with small microplates (observed on the modern EPR but not on older seafloor, presumably because of effects of sedimentation and increasing water depth on gravity anomalies), but larger microplates might be expected to be observable [e.g., *Goff and Cochran*, 1996].

The isochrons in Figure 1a are essentially as given by *Muller et al.* [1997], though with the 5, 10, and 15 Ma isochrons adjusted to be more consistent with the core data (Figure 3b). Sediment thicknesses were sampled along isochrons and converted to dry bulk mass density (mass per unit area of seafloor) to correct for compaction (Figure 4, bold lines) allowing for density variations along the equatorial zone (see caption to Figure 4). Figure 5 (bold line) shows characteristics of a Gaussian curve fitted to the data in Figure 4.

2.3. Interpretation

Figure 2 illustrates the anticipated effect of northward Pacific plate motion on the stratigraphy. The sediment isochrons represent sedimentation intervals displaced to the north by varying amounts depending on sediment age and history of plate motion, and the lower graph represents the net sediment load obtained by integrating the intervals. According to Figure 2, the sediment load should be broader than most of the individual isochrons and should be displaced northwards by an amount depending on the accumulation rates of the intervals and on the plate motion. Figures 1a and 4 (bold lines) generally show these features, with sediment thickening as far west as 35 Ma seafloor, and with the bulge displaced progressively northwards and broadening. However, there are anomalies, for example, peak thickness reaches ~500 m at 115°W but decreases below 400 m farther west before abruptly increasing again above 500 m at 130°W. This is reflected in the stepped structure of Figure 5a (bold line), which shows uniform mass on 15-25 and 35-55 Ma seafloor. The width (Figure 5c) is constant beyond 20 Ma and the center (Figure 5b) may even move southwards slightly beyond 45 Ma. The basement topography (Figure 6) shows a northward-deepening gradient for 45-65 Ma seafloor, so the westerly sediment anomaly may reflect variable carbonate dissolution with depth. Similarly, the basement depression around 2°-3°N on 25 Ma seafloor may explain the locally thin sediment there, although uncertainty in the basement age east of 125°W complicate this interpretation. The following modeling attempts to explain some of these features.

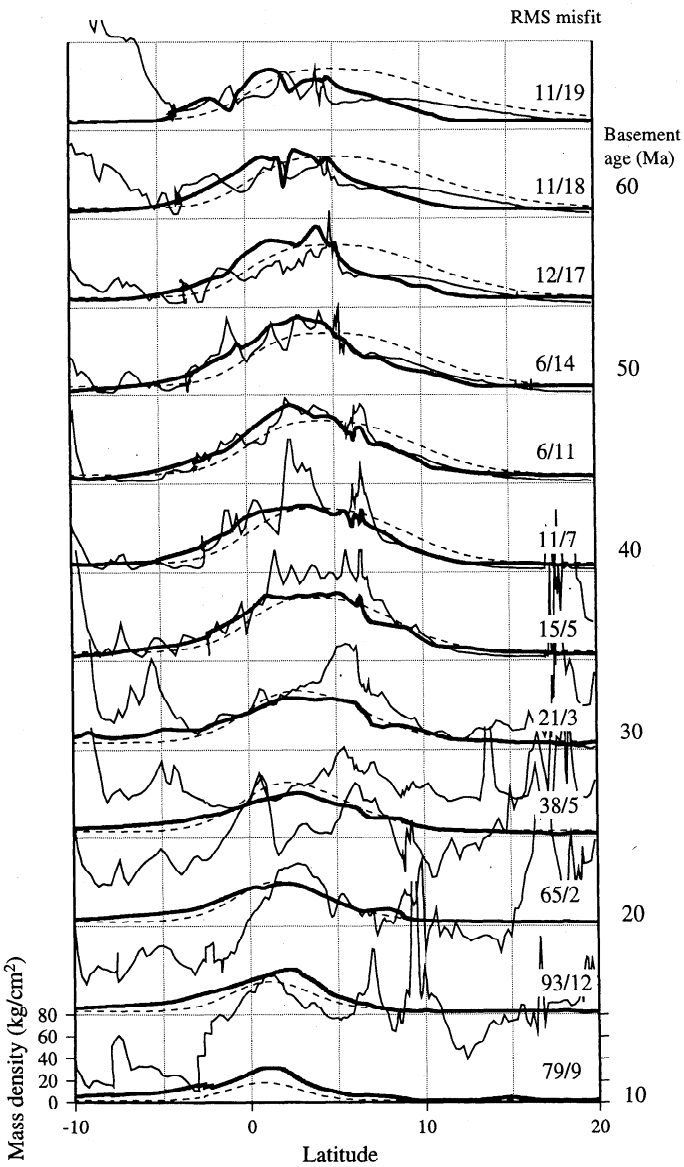

3. Sedimentation Model

The sediment distribution is simulated by backtracking individual sites across the equatorial region using a model for Pacific plate motion and summing the accumulation rates along the path, which are varied both temporally, using accumulation rates from two near-equatorial DSDP sites (Figure 7a), and with paleolatitude (Figure 7b), to simulate enhanced rates along the equator. Dissolution is also accounted for using a reported dependence of accumulation rates on depth. The model essentially involves adjusting the accumulation rates of the two DSDP sites according to the difference in paleolatitude (simulating equatorial enhancement) and according to differences in paleodepth (simulating dissolution) between the DSDP sites and a particular site being modeled. Hence the model accumulation rates can be regarded as extrapolated from the two reference DSDP sites, though using rules concerning how accumulation rates vary derived from the wider DSDP data [e.g., *van Andel et al.*, 1975].

Accumulation rates from DSDP Sites 573 and 574 (largely from hydraulic piston cores) provide the temporal variability in sedimentation. Site 573 data were used for 0-10 Ma and 574 data prior to 10 Ma, dates when these sites lay within the high-productivity zone. Bulk mass accumulation rates (MAR) were calculated from age-depth data [*Barron et al.*, 1985] adjusted to the timescale of *Cande and Kent* [1995] with dry bulk densities from *Wilkens and Handyside* [1985]. Note that the simulation

Figure 4. North-south transects for various basement ages of sediment mass density (mass per unit area, bold line) and the modeled distribution (dashed and fine lines). Sediment thicknesses have been converted to dry bulk mass density using second-order density-depth regressions. These regressions were dry bulk density $\rho=0.5443+0.00429z-0.00000550z^2$ calculated from DSDP Leg 85 Sites 573, 574, and 575 [*Mayer and Theyer*, 1985] and $\rho=0.569+0.00163z-0.00000194z^2$ from ODP Leg 138 Sites 848, 849, 850, 851, 852, and 853 [*Mayer et al.*, 1992b], where z is depth below seafloor in meters. (Before regressing, Leg 85 densities were corrected for salt content [*Boyce*, 1982] and Legs 85 and 138 densities were corrected for porosity rebound using results of consolidation tests [*Hamilton*, 1976, Table 1].) To allow for spatially varying density, the Leg 85 regressions were used west of 133°W, the Leg 138 regressions were used east of 110°W and interpolated coefficients were used between 110° and 133°W. The dashed curves show the sedimentation model results without adjustment for variable dissolution with depth. The fine lines show the model calculated using the dissolution rate gradients of *Heath et al.* [1977] but extrapolating beyond the likely lysocline depth, showing some overestimation of accumulation rates in the central region. RMS misfits to the data curves (two numbers above right of each graph) were calculated for this model with dissolution and the dashed model without dissolution, respectively. The rms values were computed over 0°-15°N after the data and model curves were averaged over ±2 m.y. seafloor and after smoothing with a 2° cosine-tapered filter to reduce the model resolution to that of the sediment thickness data.

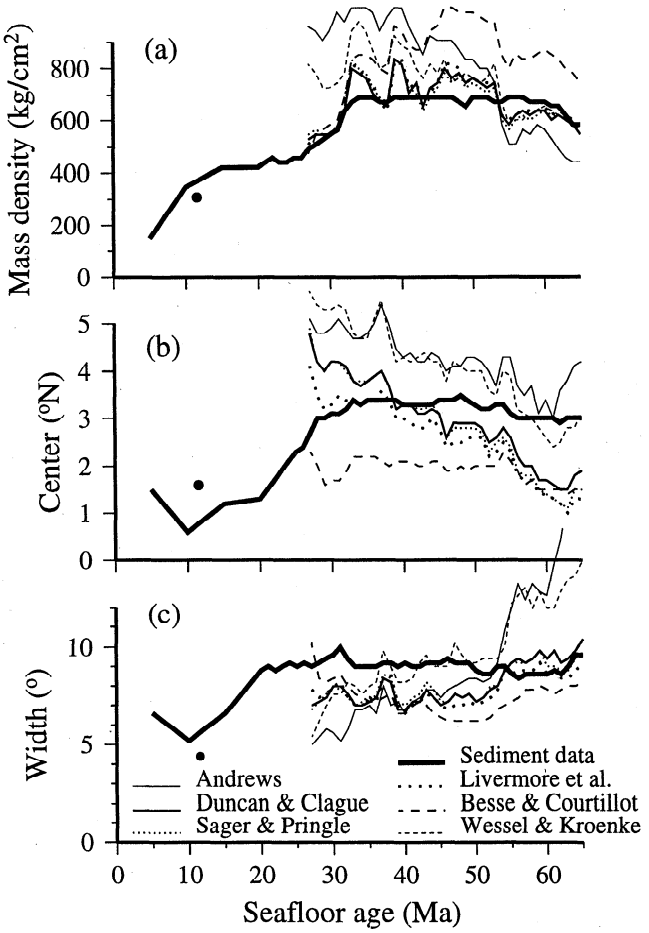

Figure 5. A Gaussian function was fitted to the isochron lines to characterize (a) the sediment load (peak height of the fitted Gaussian), (b) their centers, and (c) 2σ widths. The lines represent the data in Figure 4 (bold line) and the model sediment distribution calculated using various plate kinematic models (medium bold line, *Duncan and Clague* [1985] Pacific hotspots model; fine dashed line, *Wessel and Kroenke* [1997] Pacific hotspots model; fine dotted line, *Sager and Pringle* [1988, APWP 2] Pacific apparent polar wander path; fine line, Pacific hotspots *Duncan and Clague* [1985] followed by *Andrews* [1985] TPW model; bold dotted line, *Duncan and Clague* [1985] followed by *Livermore et al.* [1983] TPW model; and, bold dashed line, *Duncan and Clague* [1985] followed by *Besse and Courtillot* [1991] TPW model). The solid circles at 11 Ma are values from Figure A1a. Figure 5b at 35-40 Ma provides the best test of the plate and TPW models, and notably the simulation results correspond to the data reasonably well for three of the modelss [*Duncan and Clague*, 1985; *Livermore et al.*, 1983; *Sager and Pringle*, 1988].

developed below involves integrating MARs so the coarse resolution and any minor errors in Figure 7a will not greatly affect the results. The model peak accumulation rate beyond 33.5 Ma is 0.5 g/cm^2/kyr, a rough average for the Eocene [*van Andel et al.*, 1975; *Worsley and Davies*, 1979]. Only a rough value is needed here because the Eocene rates are from near the base of the cores, which may have been affected by local redistribution (sedimentation on young seafloor is highly uneven) and because the simulated sediment thickness data potentially have a post-Eocene bias as mentioned earlier. MAR is varied with paleolatitude y (Figure 7b) using the following equation which approximates the core data of *van Andel et al.* [1975].

$$m(y,t) = m_0(t)\left(0.1+0.9\ \exp\left(\frac{-y^2}{2\sigma^2}\right)\right) \quad (1)$$

The model equatorial accumulation rate $m_0(t)$ was calculated from the MARs of the two reference sites (Figure 7a) by first inverting the equation, that is, using the reference site MARs for $m(y,t)$ with their paleolatitude histories $y(t)$ calculated from the tectonic model. Equation 1 assumes that pelagic supply does not vary with longitude, so the results will become gradually less accurate away from the two reference DSDP sites due to errors in this assumption. The width parameter σ was set to 2° of latitude for 0-11 Ma (see Appendix) and 3° for older times. The latter value was chosen because it agrees with data of *van Andel et al.* [1975] and achieves a reasonable match to the width of the sediment bulge at 35-45 Ma. Interestingly, the transition at 11 Ma might relate to changes in the equatorial current system [*van Andel et al.*, 1975] but is unfortunately not well resolved in time or magnitude here. Besides the change at 11 Ma, fluctuations in width are ignored because they are not well resolved in the DSDP data (they are likely to produce little error if they are small, short-lived, or do not correlate with MAR temporal variations).

To account for dissolution, we assume the model shown in Figure 8 in which carbonate MAR varies linearly with depth between a CCD and sedimentary lysocline, and varies little above the lysocline [*Berger*, 1978]. Although the theoretical explanation for this variation is presently unclear, the relation is justified on empirical grounds because it commonly occurs in

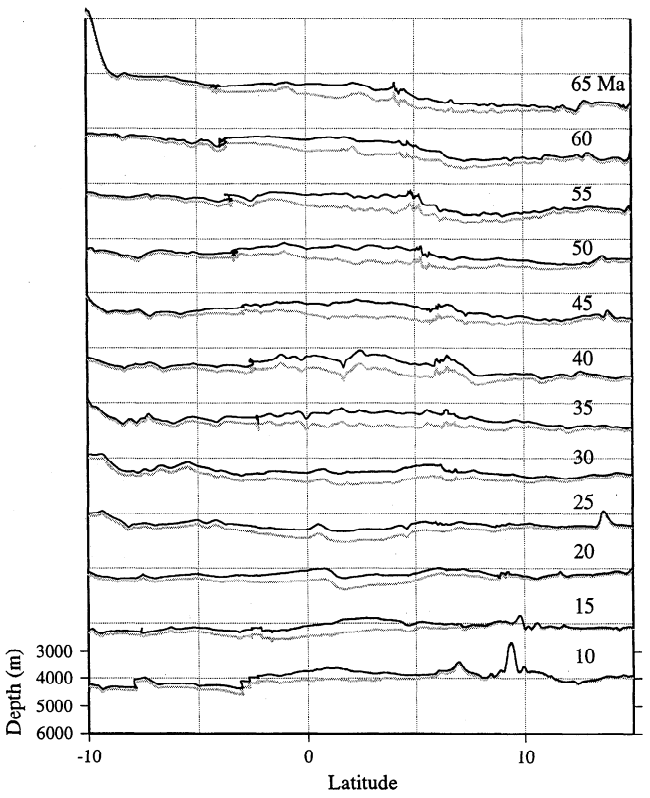

Figure 6. Bathymetry cross sections obtained by gridding all available bathymetry for the equatorial Pacific and sampling along the isochrons in Figure 1a. Sediment thicknesses were subtracted to give a rough impression of basement topography (grey lines). The horizonal dotted lines give the 4000 m depth relative to each profile.

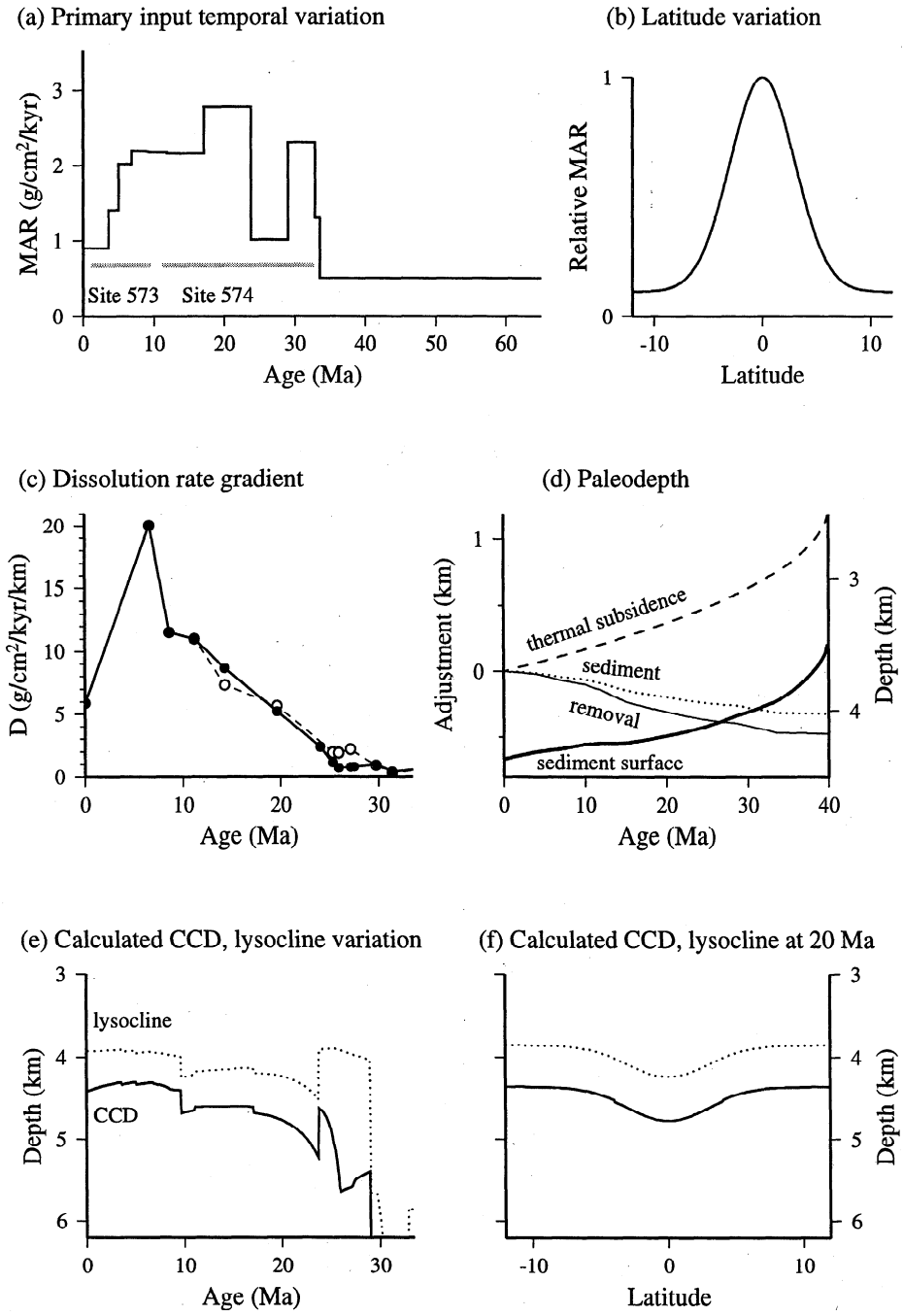

Figure 7. Forward model components. (a) Mass accumulation rates for DSDP Sites 573 and 574 based on age-depth data of *Barron et al.* [1985] adjusted to the timescale of *Cande and Kent* [1995] with dry bulk densities from *Wilkens and Handyside* [1985]. Values from 23.75 Ma to 33.5 Ma are reduced by 25% to compensate for enhanced deposition at Site 574, which was cored over a basement depression observed in seismic records [*Shipley et al.*, 1985]. The curves otherwise differ from those of *Theyer et al.* [1985] because of timescale differences and possibly because wet rather than dry bulk densities may have been mistakenly used in the original report. The rate of 0.5 g/cm^2/kyr beyond 33.5 Ma is an average value from *van Andel et al.* [1975]. (b) The MARs of Figure 7a are adjusted using this Gaussian function and the calculated paleolatitude to account for equatorial concentration of sediment supply. (c) Variable dissolution with depth is accounted for using these estimates of rate of change of carbonate MAR with depth [*Heath et al.*, 1977] and the difference in paleodepth between the backtracked site and the reference DSDP Site 573 or 574. Solid lines represent rates calculated for areas within 4° of the paleoequator and open symbols connected by dashed lines are from outside the ±4° equatorial region. Values and dates have been adjusted to the *Cande and Kent* [1995] timescale. (d) Example paleodepth calculation. The sediment surface evolution is calculated from basement thermal subsidence (dashed) and by stripping off successive surficial sediment layers (fine continuous line) allowing for isostasy (dotted line). Due to competition between thermal subsidence and sediment accumulation, the evolution for sites of thickest sediment can be significantly flatter than predicted by the subsidence alone. (e) and (f) CCD calculated from the MARs (Figures 7a and 7b) using the dissolution rate gradient in (Figure 7c) and the paleodepth evolution of the two DSDP sites. The abrupt CCD drop near 30 Ma is an artefact due to low D in (Figure 7c) while there is high MAR in (Figure 7a). The model CCD is also shallower at 25 Ma than interpreted from carbonate content in cores [*van Andel et al.*, 1975] suggesting that D in (Figure 7c) may be too high (the error is not expected to greatly affect these results though may cause a slight exaggeration of the effect of depth-dependent dissolution).

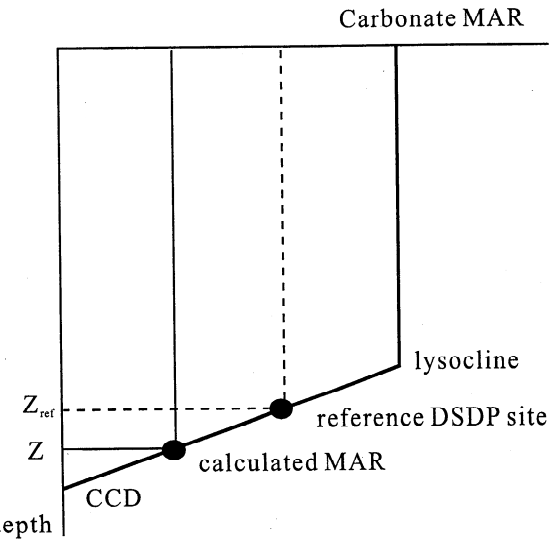

Figure 8. Dissolution model. We idealize carbonate MAR with depth as a linear variation between a carbonate compensation depth (CCD) and a sedimentary lysocline, and little variation above the lysocline (based on *Heath and Culberson* [1970]). The carbonate MAR at a location is calculated by adjusting the carbonate MAR of the reference DSDP site using the difference in paleodepth (Z-Z_{ref}) and the gradient of the graph D, which is the dissolution rate gradient (rate of change of carbonate MAR with depth) shown in Figure 7c.

modern sediments [e.g., *Berger et al.*, 1982] and carbonate MAR in DSDP cores from the central equatorial Pacific varies linearly with depth above a CCD [*Heath et al.*, 1977; *van Andel et al.*, 1975]. However, because this justification is only empirical, the model predictions may become less accurate with distance away from the center of the region (35-40 Ma seafloor) where the carbonate MARs were originally measured. The adjusted bulk MAR is given by the following equations.

$$m(t, \Delta Z) = (1-C)m(t) + Cm(t) - D(t)\,\Delta Z \qquad Z_{CCD} > Z > Z_{lysocline} \quad (2a)$$

$$m(t, \Delta Z) = (1-C)m(t) \qquad Z_{CCD} < Z \quad (2b)$$

$$m(t, \Delta Z) = (1-C)m(t) + Cm(t) + D(t)(Z_{ref} - Z_{lysocline}) \qquad Z < Z_{lysocline} \quad (2c)$$

Equation (2b) is for areas below the CCD, and (2c) is for areas above the lysocline depth $Z_{lysocline}$. C is the average carbonate fraction of the Leg 85 cores (0.798), ΔZ is the difference in paleodepth between a site Z and reference DSDP site, Z_{ref} (from the paleodepth calculation described below), and $m(t)$ is calculated from (1). $D(t)$, shown in Figure 7c, is the rate of change of carbonate MAR with depth due to dissolution measured by *Heath et al.* [1977]. The dashed curve in Figure 7c is for nonequatorial sites and was used when y was farther than 4° from the equator. Z_{CCD} is the calcium carbonate compensation depth calculated from $Z_{ref} + Cm(t)/D(t)$. Note that the coarse resolution of the MAR data and D (Figures 7a and 7c) may cause errors for areas close to the CCD or lysocline because unresolved transient periods of overestimated MAR will not be compensated by corresponding underestimated MAR and vice versa. This may partly explain poor model results for seafloor younger than 30 Ma and older than 50 Ma. Equations (1) and (2a)-(2c) assume that there is no depth-dependent loss of the noncarbonate fraction and that the noncarbonate supply varies sympathetically with carbonate. Errors in these assumptions have little effect in practice because the noncarbonate fraction is minor.

The depth of the sedimentary lysocline is poorly known for the Cenozoic equatorial Pacific [*van Andel et al.*, 1975] so two models were applied, one employing (2a)-(2c) unbounded, that is, extrapolating MARs using the slope of the carbonate MAR graph D without any lysocline, and another with the following proposed lysocline. This lysocline is constrained at recent times and outside the equatorial region, but otherwise it is relatively speculative and constrained only in the sense that it provides a more reasonable match of model to data.

$$Z_{lysocline} = Z_{CCD} - \frac{W_0}{3}\left(2 + \frac{D_0}{D(t)}\right) \quad (3)$$

The last element is the modeled width of the carbonate dissolution transition zone, where W_0 is the average transition zone for 0-800 kyr (500 m from *Farrell and Prell* [1989]) and D_0 is 5.8 g/cm^2/kyr/km, a typical dissolution rate gradient [*van Andel et al.*, 1975] for 0-800 kyr. Equation (3) was arrived at by trial and error so that the transition width is similar to that observed at 15°S for the period 0-15 Ma [*Rea and Leinen*, 1985] and also roughly bounds the linear MAR/depth data [*Heath et al.*, 1977; *van Andel et al.*, 1975]. The width of the dissolution transition zone over the past 2 Ma by *Farrell and Prell* [1991] is narrow during times of high dissolution rate gradient and broad during times of low gradient. Equation (3) assumes that this relationship existed qualitatively throughout the late Cenozoic.

The paleodepth calculation (Figure 7d) is intended to represent the evolution of the sediment surface with time and involves adjusting basement depth for thermal subsidence and removing successive surficial sediment layers, allowing for compaction and isostatic loading. The thermal subsidence rate was therefore determined first as follows. The value $0.735h$ was subtracted from the bathymetry (Figure 6) where h is sediment thickness (Figure 1) and the factor 0.735 allows for isostatic loading, assuming 1.63 g/cm^3 average sediment wet density (from DSDP Sites 573 and 574) and 3.3 g/cm^3 mantle density. Adjusted depths between 10°S and 15°N were then regressed on square root of age for the interval 25-65 Ma and constrained at zero age to a depth of 3038 m, the mean East Pacific Rise (EPR) depth from the ETOP05 database (NGDC). The 0-25 Ma interval was excluded because of uncertainties in isochrons mentioned earlier. The calculated subsidence rate, 198.5 m/Ma$^{1/2}$, is somewhat low compared to the global average 350 m/Ma$^{1/2}$ [*Parsons and Sclater*, 1977], but it is consistent with the global tendency for subsidence rate to be lower for deep ridge axes [*Kane and Hayes*, 1994] given the deep EPR axis here. Paleodepth is therefore given by

$$Z(t) = Z_0 + I(h_0) - I(h(t)) - 198.5(\sqrt{a} - \sqrt{(a-t)}) \quad (4)$$

where Z_0 is the present depth at a site, h_0 is the present thickness at that site, and a is basement age. $I(h)$ is the effect of sediment thickness adjusted for isostatic loading according to the mean sediment density expected for that thickness and site longitude (i.e., allowing for regional density variations). To allow for varying sediment thickness with time, we scale the mass at a site M_0 according to the predicted MAR temporal variation:

$$h = h\left(M_0 . \frac{M(a) - M(t)}{M(a)}\right) \quad (5)$$

where $M(t)$ is the time integral of (1) and $h(M)$ is in practice a

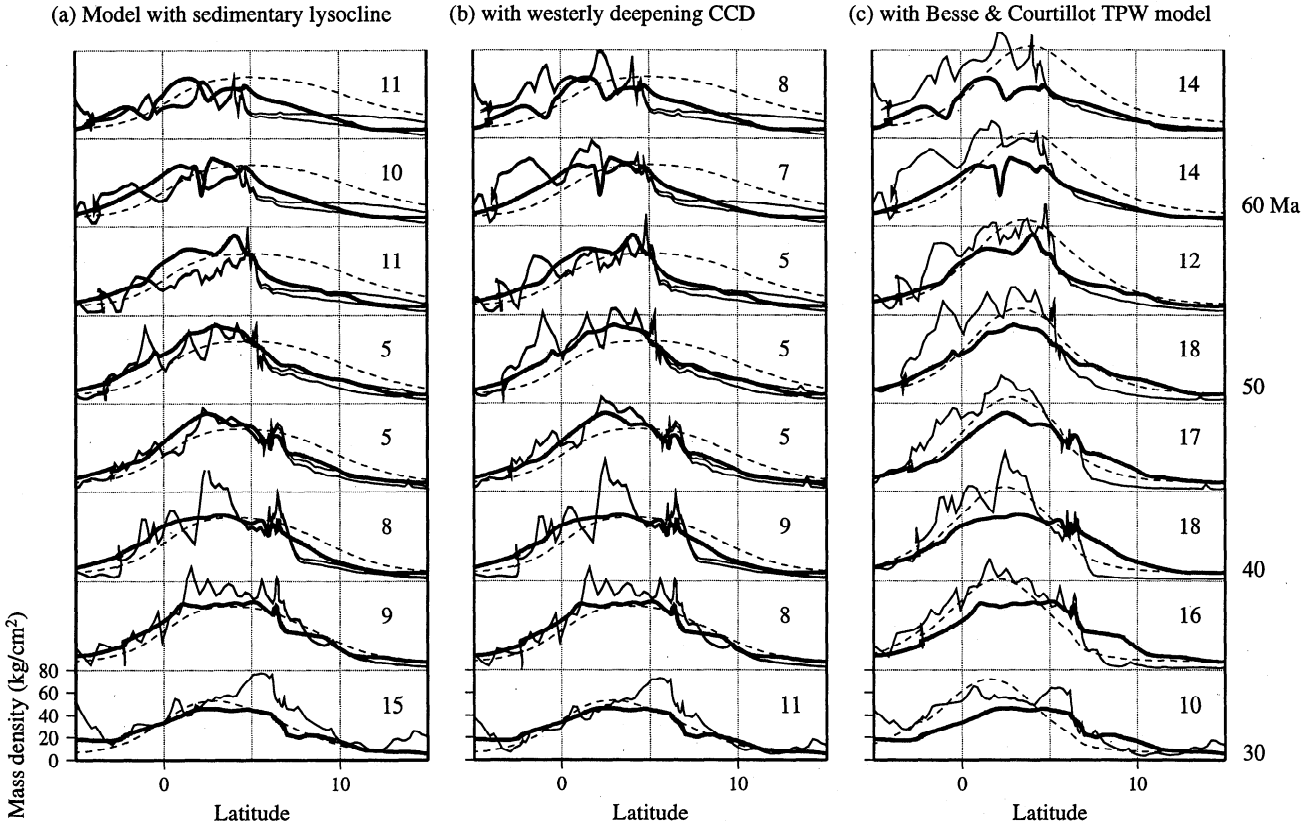

Figure 9. (a) The two fine lines in each profile show the forward model refined by including a sedimentary lysocline. The lower of the two lines was calculated with no sedimentation before 33.5 Ma to simulate the sediment thickness data if biased by reflective Eocene cherts. (b) As Figure 9a but also with a CCD deepening to the west by 10 m per degree of longitude. (c) As Figure 9b, including pre-33.5 Ma sediments, calculated with an alternative kinematic model. Backtracking was calculated using a Pacific hotspots model [*Duncan and Clague*, 1985] combined with the true polar wander model of *Besse and Courtillot* [1991]. Because of slow movement of the paleoequator in this model (Figure 11b), the predicted sediment distribution is more concentrated than the data. The better match of Figure 9b to the sediment distribution therefore favors TPW models which have little effect on the central Pacific paleoequator in the period 0-30 Ma. The rms misfits to the data curves (numbers above right of each graph) were calculated for the model with dissolution over 0°-15°N. The rms values were computed after the data and model curves were averaged over ±2 m.y. seafloor and after smoothing with a 2° cosine-tapered filter to reduce the model resolution to that of the sediment thickness data.

look-up table which returns the sediment thickness corresponding to M. The table is intended to compensate for sediment compaction and uses the density/depth regressions described in the caption to Figure 4. By using the accumulation rate history, the paleodepth calculation includes distortion caused by drift relative to the equatorial productivity zone, although it may still leave some minor paleodepth errors if there are substantial hiatuses or if areas crossed the CCD. Paleodepths for the two reference DSDP sites were calculated as above except that depth down core for Site 574 was calculated using the MARs for that site rather than the combined model in Figure 7a.

4. Inferences on the Pacific Sedimentary System

To illustrate the different stages in developing the above model, Figures 4, 9a and 9b show output of four models: without dissolution (dashed curves in Figure 4), with dissolution but without a lysocline (fine lines in Figure 4), with a lysocline (fine lines in Figure 9a) and with an east-west CCD gradient (fine lines in Figure 9b). These models were calculated using the Pacific apparent polar wander path (APWP) of *Sager and Pringle* [1988]. Because of the geometry in Figure 2, the 2°-4° uncertainty in the 39 Ma pole of *Sager and Pringle* [1988] leads to a ~1°-2° uncertainty in the modeled sediment deposits.

In order to illustrate how dissolution modifies the shape of the sediment bulge, Figure 4 compares the sediment thickness data (heavy solid curves) to a model without dissolution (dashed curves), which is essentially obtained by integrating the MARs modified only by the latitude variation (equation (1)). The curves match the data roughly in terms of center for 20-30 Ma, height for 35-65 Ma, and width at 35 Ma, which is the basement age around Sites 573 and 574. The basement topography is regionally flat along the 35 Ma transect, suggesting little differential dissolution, so this match generally supports the chosen latitudinal variation (Figure 7b). Although this model is incomplete, the rms misfit values (the second numbers on the right of Figure 4) show a better match of this model to the data for 10-40 Ma than the following models with varying carbonate dissolution with depth, which could indicate that the dissolution is less sensitive to depth in this easterly area. In detail, the model differs from the data in a number of areas. Peak sediment mass is slightly overpredicted for 25-30 Ma, the region of anomalously thin sediment in Figure 1a.

Interestingly, the model for 40-65 Ma seafloor overpredicts mass north of the bulge at 10° N and underpredicts south of the bulge at 0° N. Figure 6 shows a basement depression at the equator for 25 Ma seafloor and a regional northward-deepening basement gradient for 50-65 Ma seafloor so some of these features may be caused by variable carbonate dissolution with depth.

When dissolution is included (fine lines in Figure 4), bathymetry variability results in a model that is noisy, and the lack of a lysocline causes overprediction of the sediment mass in some areas. The model is greatly in error for 10-25 Ma seafloor, and for many areas south and north of the equatorial zone for 10-30 Ma. Despite the variability, however, the model center corresponds to the data better for 40 Ma seafloor. This seafloor lies in the center of the region over which DSDP data were used to derive the width parameter σ and dissolution rate gradients D [*van Andel et al.*, 1975] and close to the two reference DSDP sites. Compared to the model without dissolution, this model shows that the greater mass south of the bulge and missing mass north of the bulge could both be caused by varying dissolution with depth over a regional basement gradient (Figure 6). The northerly missing mass has previously been attributed to dissolution and erosion by bottom currents locally north of the Clipperton fracture zone [*Johnson*, 1972b], whose relief may have constrained bottom current flow [*Johnson*, 1972a]. Although there is strong evidence for hiatuses [*van Andel et al.*, 1975], these model results suggest that dissolution might be better described as causing a regional distortion of the sediment bulge.

The pairs of fine lines in Figure 9a show model runs including the lysocline calculation (equation (3)). The lower of each pair of curves represents sediment mass deposited 0-33.5 Ma, simulating the deposits (Figure 1a) if biased by reflective Eocene cherts. The model is slightly improved compared to Figure 4 for 30-40 Ma seafloor, as shown by the rms misfit values (numbers to right of each graph in Figure 9a), although it is still in error beyond the central 30-40 Ma region. The overprediction for seafloor of 30 Ma and younger might be partly due to paleodepth errors, which are greatest near the base of the sediment section [*Berger*, 1973] (subsidence rates are highest for younger seafloor during the time of high MAR and D in the model), but differences between DSDP Sites 572 and 573 (at 114°W and 133°W, respectively) suggest the mismatch is more likely due to longitudinal variations in dissolution conditions, sediment composition and supply rates as described by *Theyer et al.* [1985]. If correct, Figures 9a and 1a suggests that the transition occurs between 25 and 30 Ma seafloor, or 124°-129°W.

The model for seafloor of 55 Ma and older in Figure 9a has two areas of excessive dissolution, within 0°-4°N and 6°-8°N. Both are probably due to a westwardly deepening of the CCD which is not included in the model (although the paleodepth calculation differs from *Berger and Winterer* [1974] and *van Andel et al.* [1975], this is unlikely to have caused the error because the subsidence rate used here is at the lower extreme of global values). In the model calculation for Figure 9a, DSDP Site 72 (0° 26.5'N) on 55 Ma seafloor lies below the CCD for 0-10 Ma, while Site 72 cores show carbonate during this interval [*Tracey*, 1971]. To simulate a westerly deepening CCD, Figure 9b shows the distribution predicted by offsetting the bathymetry by 10 m per degree of longitude from 133°W. Although still underpredicting the sediment mass north of 5°N for 55-65 Ma seafloor, the results are improved for 55-60 Ma seafloor, suggesting there has been a regional CCD gradient of ~10 m/° for much of the upper Cenozoic.

A distortion remains in the model for 50-65 Ma (Figure 9b), with excess mass south of the equator and underestimated mass north of 5° N, but its origin is unclear and in any case the seismic coverage (Figure 1b) is poor on the south side of the bulge. The following test of plate models therefore uses the degree of match for 30-45 Ma seafloor where the sedimentation model is more accurate.

5. Plate Kinematic Models and True Polar Wander

For the purpose of resolving the northward drift of the Pacific plate, we ran the sedimentation model described above using different plate motion models. Figure 10a shows the model results averaged over seafloor between 30 and 45 Ma. The

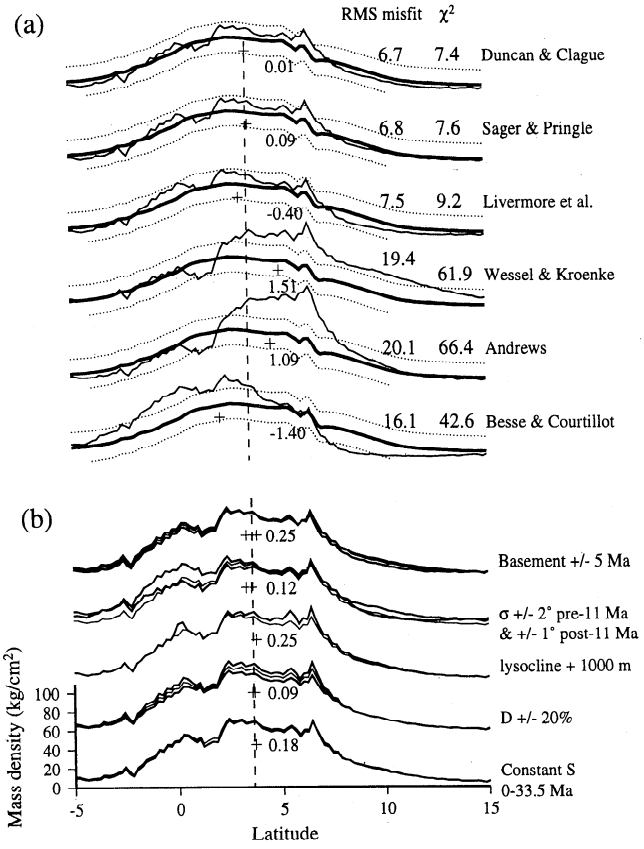

Figure 10. (a) The mean sediment distribution for 30-45 Ma seafloor (bold) compared to model results (fine lines) calculated using different plate motion models. The vertical dashed line is the center of mass (COM) of the data calculated over 5°S to 15°N. The pluses and associated values show the corresponding model COM and deviation from the data COM. The rms misfits and χ^2 estimates (above right values) were also calculated over 5°S to 15°N. The dotted lines show the effect of all uncertainties in sedimentary model parameters and sediment thickness measurements (plotted as a combined error about the data curve to facilitate comparison). (b) Illustration of the effect of various model parameter uncertainties on the COM. Models were run using the *Sager and Pringle* [1988] APWP and with dissolution as described in the text for Figure 9b. The pluses and associated values show the change in the COM caused by the changes in model parameters shown. The model is insensitive to dissolution parameter uncertainties because the basement topography is regionally flat for 30-45 Ma seafloor (Figure 6).

accuracy of the plate model can be assessed from how well it predicts both the center of mass (COM) and the shape of the sediment bulge, illustrated by the rms misfits and by a χ^2 misfit test. The sedimentation model is most accurate for 30-45 Ma seafloor because the two reference DSDP sites lie in the center of this area and 30-45 Ma seafloor lies within the broader region over which the dissolution rate gradients D and width parameter σ were measured from DSDP data.

5.1. Error assessment

5.1.1. Center of mass. We assess the accuracy of the comparison between the COM of the data and models by considering the effects of uncertainties in the various sedimentary parameters, the sediment thickness map, and in the extent to which sedimentation is centered on the equator. In the conceptual model (Figure 2), the center of the bulge is displaced north of the equator by roughly half the total plate motion that occurred over the late Cenozoic period of rapid sedimentation (0-33.5 Ma). Thus, the uncertainty in the total plate motion constrained by the modeling will equal roughly twice the uncertainty in the data/model COM comparison. This error assessment assumes that the plate motion is relatively steady and that its magnitude predicted with the *Sager and Pringle* [1988] poles is correct to within a few degrees. Note also that we do not include uncertainties in the plate motion itself because the data/model COM comparison is intended to test the plate motion models. The effect of uncertainties in the sedimentary model parameters is illustrated in Figure 10b. The graphs show the average sediment mass distribution for 30-45 Ma seafloor modeled with the *Sager and Pringle* [1988] poles and incorporating dissolution as described for Figure 9b. The pluses and associated values show the movement of the COM caused by adjusting the sedimentary parameters as shown on the right of Figure 10b. The choice of the parameter uncertainties is as follows.

Basement age at DSDP Sites 573 and 574 [*Mayer and Theyer*, 1985] agree with the age grid [*Muller et al.*, 1997] to within 2.5-3.2 and 1.3-2.4 m.y., respectively (Figure 3b). Given also the isochron uncertainties described earlier, we chose an uncertainty in the average age of the 30-45 Ma region of 5 m.y. Figure 10b shows the effect of offsetting all basement ages by ± 5 m.y. The model output is insensitive to basement age uncertainty where basement is older than the post-Eocene period of rapid sedimentation (0-33.5 Ma).

The appendix describes how a maximum uncertainty in width parameter σ was derived for 0-11 Ma sedimentation. The width is more poorly constrained for the older sediments, and the value for σ estimated from the graphs of *van Andel et al.* [1975] could potentially be in error by up to 2°. The curves in Figure 10b were calculated by adjusting σ by 1° for 0-11 Ma and 2° for pre-11 Ma.

We adjusted the model lysocline by 1000 m to provide a maximum estimate of the uncertainty because of the lack of paleobathymetry above this level. D was originally measured by graphing carbonate accumulation rates against depth for various time intervals. Given the distribution of data given by *van Andel et al.* [1975, Figure 60] and *Heath et al.* [1977, Figure 4], individual measurements of D could have been in error by up to 20%. We varied all the values of D by 20%, which will give a conservative error estimate because errors are likely to be uncorrelated between estimates of D for different ages. Both dissolution parameter uncertainties (lysocline depth and D) produce relatively little effect on the model COM (Figure 10b) because the regional basement topography is relatively flat for 30-45 Ma seafloor (Figure 6).

The sediment accumulation rates in Figure 7a could be unrepresentative of the bulge as a whole because of local sedimentary processes (local downslope movements or variable effects of bottom currents). To provide a rough error estimate, we averaged the accumulation rates between 0 and 33.5 Ma in Figure 7a and ran the model to produce the bottom curve in Figure 10b. The effect is minor because the model involves integrating the accumulation rates. A significant effect on the model COM would only occur if the rates in Figure 7a had a strong systematic error with age, but the general decline from 20 Ma to present is compatible with the general trend observed from all the older equatorial DSDP cores [*van Andel et al.*, 1975].

Uncertainties in the sediment data COM (dashed line in Figure 10a) are caused by inadequacies in the data coverage (Figure 1b) and problems with interpreting original oceanic basement from the seismic data. Sills and flows around the "crossgrain" volcanic ridges [*Winterer and Sandwell*, 1987] in particular complicate the interpretation. We assume that seismic masking could potentially have obscured up to ~150 m of sediment (~20 kg/cm^2) over a region of 2° of latitude and over the total width of the 30-45 Ma region. Such a bias in the mass distribution would offset the COM by 0.7°.

A further uncertainty concerns the extent to which the zone of high productivity has been centered on the equator throughout the late Cenozoic. Present-day maximum productivity occurs on the equator, but north of the equator the productivity is generally higher than for similar latitudes south of the equator [e.g., *Pena et al.*, 1990]. The 0.7°N center for 0-11 Ma sedimentation derived in the Appendix may reflect this asymmetry. Furthermore, hiatuses are more common in drill cores north of the equator which may reflect greater bottom current activity and corrosive effects on carbonates [*van Andel et al.*, 1975]. While differential chemical erosion of carbonates is partly accounted for in the model by varying dissolution northward over the regional bathymetric gradient, there may be some unaccounted anomalies. We suggest that a full 1° uncertainty in latitude should be added to the error budget to account for these uncertainties until they can be more accurately estimated.

We combined the uncertainties by assuming that the sedimentary parameter and thickness data uncertainties are all uncorrelated so they should be added as the sum of the squares (giving a net uncertainty of 0.82°). The uncertainty in the productivity center should be added as a systematic error, giving a total uncertainty of 1.8°. The accuracy with which the modeling constrains the post-Eocene paleolatitude drift is twice this value, that is, 3.6°.

5.1.2. Curve mismatch. To assess the accuracy of the models in Figure 10a, we calculated the statistic

$$\chi^2 = \sum_{i=1}^{N} \left(\frac{M_0(y_i) - M_m(y_i)}{\sigma_i} \right)^2 \qquad (6)$$

where $M_o(y_i)$ and $M_m(y_i)$ are the measured and modeled sediment mass per unit areas at latitude y_i and σ_i are the combined uncertainties. The spacing of independent values in Figure 10a is assumed to be 0.5° of latitude based on the distribution of seismic data used to construct the sediment thickness map and based on the distribution of other data used in the modeling. The uncertainties σ_i cannot be estimated easily for each latitude y_i

because the model sediment mass uncertainty itself depends on the paleolatitude history of the Pacific plate. We therefore instead estimate an average uncertainty and use it for all σ_i in (6). Although not strictly correct, the values for χ^2 will nevertheless provide an approximate guide to the goodness of fit and the σ_i are in any case dominated by the uncertainty in picking basement from seismic records, an error that is not expected to vary much with latitude.

The effect of the model uncertainties in Figure 10b was assessed by calculating the mean error magnitude for each graph and combining these as the sum of the squares. Bathymetry errors may also distort the modeled sediment distribution, by erroneous modeling of dissolution, but this requires that the bathymetry has a systematic error with latitude. We suspect these effects are minor because of the high density of ship tracks (~2000 soundings per 0.5° of latitude for 30-45 Ma seafloor). However, in order to have a conservative error estimate, we assume a bathymetry uncertainty of 50 m and ran the sedimentation model as described above for Figure 10b with a depth offset of 50 m (producing an average uncertainty of 4 kg/cm^2). The largest remaining uncertainty is that related to picking acoustic basement from the seismic records. Considering the density of lines in Figure 1a, we believe a rough value of 0.1 s (two-way time) is a reasonable average uncertainty for the mean thickness over regions of 0.5° of latitude covering 30-45 Ma seafloor. This leads to an uncertainty in the sediment mass of 13 kg/cm^2. The net error due to all these factors combined is 15.6 kg/cm^2, which is illustrated by the dotted lines in Figure 10a. The critical value for χ^2 (95% confidence level) is 59 assuming 40 degrees of freedom. This suggests that the first three and last one model curves in Figure 10a are acceptable within the uncertainties, but the fourth and fifth models (labeled Wessel & Kroenke and Andrews) are not acceptable.

5.2. Results

The main result from the center of mass assessment in Figure 10a is that the Pacific plate drift has been 9.2°±3.6° over the past 33.5 m.y. (*Cande and Kent* [1995] timescale). This figure was derived from the 9.4° post-Eocene motion predicted using the 39 Ma pole of *Sager and Pringle* [1988], adjusted by 0.2° to allow for twice the 0.1° discrepancy between the data and model COMs in Figure 10a. More complicated drift histories represented by the bottom three graphs in Figure 10a are not excluded on the basis of the COMs because they fall within the conservative uncertainty ranges, but we still consider these to be unlikely because they are inconsistent with the equator crossings interpreted from drill cores (horizontal bars in Figure 11b) and they predict anomalous mass distributions, described as follows.

Figure 11b shows paleolatitude evolution for a site presently at 5°N, 145°W predicted with alternative models for Pacific plate motion. The bold continuous, dot-dashed and fine dashed lines in Figure 11b were obtained by backtracking using the models for Pacific plate motion relative to hotspots of *Duncan and Clague* [1985], *Cox and Engebretson* [1985], and *Wessel and Kroenke* [1997], and the fine dotted line using the apparent polar wander path of *Sager and Pringle* [1988, APWP 2]. The other curves were calculated by backtracking using the Pacific hotspots model of *Duncan and Clague* [1985] and then applying a rotation to account for motion of the hotspot frame according to the true polar wander models in Figure 11a. The *Duncan and Clague* [1985], *Sager and Pringle* [1988], and *Livermore et al.* [1983] models produce a similar paleolatitude evolution for 0-40 Ma, the period of highest accumulation rates, so sedimentation models calculated from them are similar (Figure 10a). The divergence between the curves calculated from *Duncan and Clague* [1985] and *Sager and Pringle* [1988] prior to 40 Ma is due to the backtracked site passing close to the 42-65 Ma pole of *Duncan and Clague* [1985] and due to possible TPW in the model of *Sager and Pringle* [1988]. This divergence produces slightly different modeled deposits at ~10°N, which unfortunately cannot be distinguished here because of uncertainties over the extent to which Eocene and Paleocene sedimentation was focused on the equator [*van Andel et al.*, 1975] and possible post-Eocene bias in Figure 1. A map of seismically reverberant layers given by *Houtz and Ludwig* [1979], probably corresponding to pre-Oligocene sediments, shows accumulations southeast of Hawaii, so a reevaluation may help to resolve this issue if seismic data can be collected with better resolution.

The TPW paths of *Besse and Courtillot* [1991] and *Andrews* [1985] predict a slow moving paleoequator between 10 and 30 Ma (Figure 11b). Due to the static equator at 10-30 Ma predicted using *Besse and Courtillot* [1991], the modeled sediment mass is anomalously high and narrow, and the center lies farther south than the data on 30-45 Ma seafloor (Figure 9c). Similarly, the *Andrews* [1985] model predicts anomalously thick deposits centered too far north. Although the anomalous COM location produced with these two models is within the margins of uncertainty (2°), the models predict unsatisfactory shapes of the sediment bulge (Figure 10a). The χ^2 test suggests that the model based on the *Andrews* [1985] TPW motions should be rejected, while that based on *Besse and Courtillot* [1991] is marginally within the uncertainties. While the test does not formally reject the model based on *Besse and Courtillot* [1991], the model predictions are beyond the uncertainties for more than ~5° of latitude so it is still considered to be unlikely. Therefore, assuming that the *Duncan and Clague* [1985] poles adequately represent Pacific-hotspots motion (discussed below), the sediment modeling favors TPW models which have little effect on the central Pacific paleoequator, in practice favoring those TPW paths which lie close to the 146°-326° great circle at 15 Ma and 157°-337° great circle at 30 Ma.

6. Discussion

6.1. CCD and Midplate Swells

The northward-deepening basement topography (Figure 6) is associated with midplate swells, in particular that due to the Marquesas hotspot south of the equator [e.g., *McNutt and Fisher*, 1987; *Stein and Stein*, 1993]. The reasonable match of the model to data (Figure 9b), reflecting distortion of the sediment bulge by variable dissolution, implies persistence of this topographic gradient, and hence regional effects of plumes, throughout much of the late Cenozoic. However, a remaining anomaly in Figure 9b (overprediction south of 0°N and underprediction north of 5°N for 55-65 Ma seafloor) may represent an exaggeration of the bathymetry effect. Recently released gravity field images [*Sandwell and Smith*, 1997] show no trace of the Marquesas seamount chain northwest of 7°S, 142°W, suggesting that hotspot volcanism dates to no more than 10 Ma [*Duncan and Clague*, 1985]. The sediment anomaly could therefore reflect growth of the Marquesas swell. This is speculative due to the weak data distribution (Figure 1b) and possibility of regionally varying dissolution conditions, but it would be interesting to find out if collecting further drill cores south of the sediment bulge would

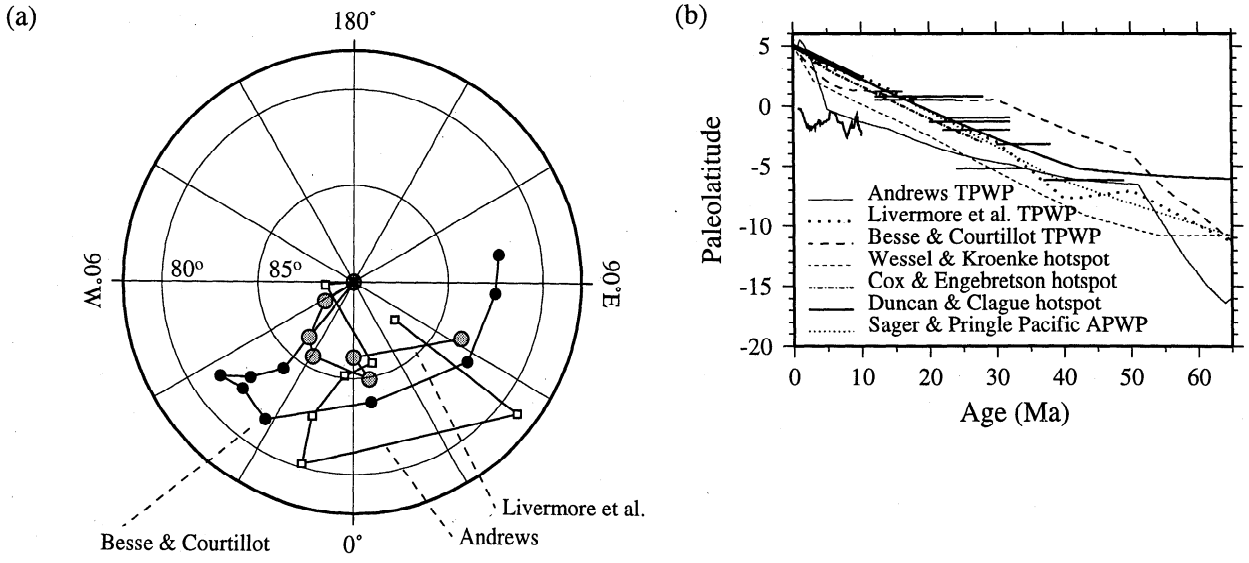

Figure 11. (a) Comparison of three models for true polar wander (hotspot frame relative to the Earth's paleomagnetic axis) for 10, 20, 30, 40, 50, 60, 70, 80, and 90 Ma (solid circles [*Besse and Courtillot,* 1991]), at 10, 20, 30, 40, 50, and 70 Ma (grey circles [*Livermore et al.*, 1983]) and at 1, 5, 14, 32, 51, 64, and 83 Ma (open squares [*Andrews*, 1985]). (b) Paleolatitude evolution predicted for various plate kinematic and TPW models for a site initially at 5°N, 145°W. The medium bold continuous, dot-dashed and fine dashed lines were obtained by backtracking using Pacific hotspots models of *Duncan and Clague* [1985], *Cox and Engebretson* [1985, poles A and D] and *Wessel and Kroenke* [1997], and the fine dotted curve using the apparent polar wander path of *Sager and Pringle* [1988, APWP 2]. The other curves were calculated by first backtracking using the Pacific hotspots model of *Duncan and Clague* [1985] and then applying a rotation to account for motion of the hotspot frame [*Andrews*, 1985; *Besse and Courtillot*, 1991; *Livermore et al.*, 1983], which is achieved by applying the rotation, with a pole in the equatorial plane, that will return the TPW path (TPWP) to the geographic north pole. The irregular line for 0-10 Ma shows the paleolatitude evolution of an equatorial site at 110°W estimated by fitting a Gaussian curve to the variation of MAR with latitude in ODP Leg 138 cores (Figure 12) and plotting the Gaussian center with negative latitude. The heavy bold line shows present Pacific motion relative to the lithosphere no-net rotation reference frame [*Larson et al.*, 1997] shown for 5°N, 145°W and extrapolated to 10 Ma. Horizontal bars show the age ranges of equatorial crossings in DSDP cores compiled by *Sager* [1984, Table 3]. To facilitate comparison with the models, the latitude of each drill site was subtracted from 5°N. The DSDP sites are 572, 166, 574, 315, 71, 69, 70, 167, 165, 161, and 163 in order of increasing present-day latitude (decreasing paleolatitude in the graph). Sites 574 and 315 have coincident latitude. Note that in Figure 11a two of the TPW models [*Andrews*, 1985; *Besse and Courtillot*, 1991] have a component that is transverse to the 150°-330° great circle, so they have a significant effect on paleolatitudes in the central Pacific. The Pacific hotspots model of *Wessel and Kroenke* [1997] predicts an abrupt paleolatitude change during 0-3 Ma which would have displaced the bulge farther north than observed, and therefore, if the Pacific hotspots motion is correct, this suggests a compensating component of TPW. The other three models predict similar paleolatitude evolutions and adequately model the observed sediment distribution. The standard errors are ~2% of latitude change for Pacific hotspots motion to 42 Ma [*Duncan and Clague*, 1985], 2°-4° for the Pacific APWP at 39 and 66 Ma [*Sager and Pringle*, 1988], and generally 4°-5° for the TPW models [*Andrews*, 1985; *Besse and Courtillot*, 1991; *Livermore et al.*, 1983].

allow us to map the evolution of the regional CCD and reveal the swell evolution. Increasing uplift due to the Marquesas swell with time should be represented by anomalously elevated CCD in older sediments immediately north of the swell compared to adjacent sites of similar latitude and age.

The deepening of the CCD by ~10 m per degree of longitude suggested by this modeling is comparable to the present-day CCD gradient of ~10-20 m per degree estimated from *Berger et al.* [1976]. This implies that east-west variations in dissolution rates, which control the CCD level, probably persisted for much of the late Cenozoic. The alternative, variation in supply, is unlikely because silica (assumed to mimic carbonate supply) shows little east-west variation during this period [*Leinen*, 1979] and opal accumulation during the last few million years had an eastward-increasing gradient [*Farrell et al.*, 1995], not a westward gradient as would be needed to explain the CCD variation. *Lyle* [1992] suggested that the presently shallow CCD in the east Pacific reflects acidity caused by degradation of organic matter supplied from or near to the American continents. The central equatorial Pacific has maintained a relatively constant distance from the continents during the late Cenozoic because subduction along the east Pacific margin has compensated for East Pacific Rise spreading [*Engebretson*, 1985], so the CCD gradient might represent a persistent effect of organic input.

6.2. True Polar Wander and Pacific Plate Motion

Differences between the TPW models (Figure 11a) probably reflect different criteria applied in selecting paleomagnetic poles [*Harrison and Lindh*, 1982]. This could explain differences between the *Andrews* [1985] and *Besse and Courtillot* [1991] models, which were otherwise calculated with similar methods. *Livermore et al.* [1983] and *Sager* [1984] discuss the further

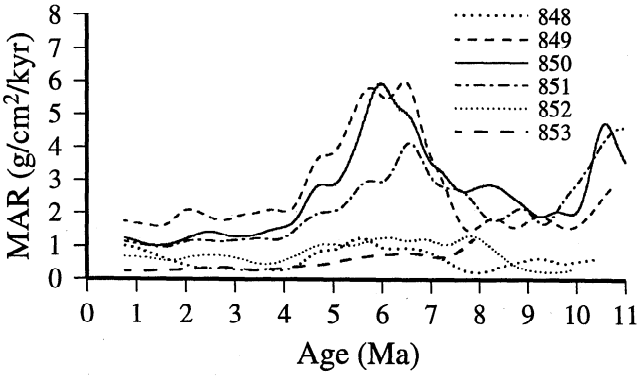

Figure 12. Bulk mass accumulation rates for the 110°W ODP transect. MARs were calculated by combining a revised stratigraphy [*Shackleton et al.*, 1995] with corresponding dry bulk densities [*Mayer et al.*, 1992b].

problem of nondipole components of the geomagnetic field which may have biased the results of *Andrews* [1985] and *Besse and Courtillot* [1991] since they excluded Pacific data, although *Acton and Gordon* [1994] argue that nondipole components should have a minor effect. A further interesting possibility is that differences may reflect relative motion between hotspots, in particular between those in the Pacific and elsewhere [e.g., *Molnar and Stock*, 1987]. The TPW model of *Livermore et al.* [1983] would therefore lie closer to the north pole because it is formed from a global data set which averages some of this motion. This could also explain the discrepancy between results from the Pacific which suggest a lack of hotspot motion [*Gordon and Cape*, 1981; *Sager*, 1984; *Suarez and Molnar*, 1980; and results herein] and those TPW models based on data from outside the Pacific basin [*Andrews*, 1985; *Besse and Courtillot*, 1991]. Motion between the Pacific and other hotspots is difficult to assess more directly, however, because of uncertainties in plate reconstruction circuits due to unresolved motion across Antarctica and elsewhere [*Acton and Gordon*, 1994], and this complicates the accurate resolution of global TPW. Although global TPW is unresolved for the late Cenozoic, we note that data from the Hawaiian volcanic chain dominate the *Duncan and Clague* [1985] Pacific hotspot model, so the lack of TPW deduced from this sediment model and from paleoequators [*Gordon and Cape*, 1981; *Sager*, 1984; *Suarez and Molnar*, 1980] imply that the Hawaiian hotspot itself has maintained relatively constant latitude after the Eocene.

Our proposed lack of TPW effects relies on an assumption of steady Pacific hotspots motion implicit in the poles of *Duncan and Clague* [1985]. However, several authors have suggested that the recent bend in the Hawaiian volcanic chain may indicate a change in Pacific hotspots motion within the last 5 m.y. [e.g., *Cox and Engebretson*, 1985], and further irregularities in the chain may reflect other unsteady motions. While the poles proposed by [*Cox and Engebretson*, 1985] predict a similar paleolatitude evolution at 145° W to that calculated from the poles of *Duncan and Clague* [1985], and hence are indistinguishable using the sediment distribution, some authors have proposed a more abrupt motion [e.g., *Wessel and Kroenke*, 1997]. The paleolatitude evolution predicted using the *Wessel and Kroenke* [1997] poles (Figure 11b) lies 3°-4° south of the other paleolatitude predictions, and the sediment mass predicted using these poles and assuming geographically fixed hotspots is unsatisfactory (Figure 10a). To further test Pacific motion, we fitted a Gaussian curve to the MAR versus latitude data from the ODP Leg 138 sites at 110°W (Figure 12) to estimate the paleoequator location. The irregular line at 0-10 Ma in Figure 11b shows the estimated paleoequator displayed with negative latitude for comparison. (The three central drill sites have similar depths, within 79 m, so the MAR trends should not be greatly affected by differences of dissolution.) Despite the variability, due to the limited number of cores, the data are more consistent with a steady ~0.1°/m.y. change of paleolatitude than one with an abrupt change in the past 5 m.y. The sediment data might be reconciled with abrupt plate motion if enhanced sedimentation had been persistently offset from the equator at 135°-145°W but not at 110°W. However, while the equatorial belt of high sedimentation is presently deflected southwards east of the Galapagos islands due to interaction with the Peru current [e.g., *Moore et al.*, 1973], there is no obvious reason to expect persistent deflection in the central Pacific. Alternatively, a 3-0 Ma pole may satisfy the Hawaiian bend and the central (135°W) and eastern (110°W) sediment distributions if it were located much farther west, such as at 50°N, 100°W, but such a pole would be inconsistent with *Wessel and Kroenke*'s [1997] interpretation of the hotspot location at the end of the Louisville chain and the 315° orientation of the Marquesas chain. Obtaining further seamount and sediment data is important for resolving this discrepancy because abrupt Pacific plate motion, which is not reflected in the sediments, might indicate a coincident, opposite effect of true polar wander of ~200 km within the last few million years. Interestingly, Figure 11b shows that the present-day motion of the Pacific plate relative to the lithosphere no-net rotation reference frame (LNNR, bold line for 0-10 Ma) is coincident with the long-term motion of the Pacific plate relative to the Pacific hotspots (medium bold line from *Duncan and Clague* [1985]). Therefore, if motion between the Pacific and surrounding plates, and between the Pacific plate and the hotspots, has abruptly changed within the last 3 m.y. [*Wessel and Kroenke*, 1997], that motion may also require motion between the LNNR frame and the hotspots. This question will require more data on hotspot motions than presently available but, if it turns out to be significant, relative motion could imply that either the LNNR or the hotspots are unsuitable references to represent the bulk Earth and therefore for resolving TPW.

7. Conclusions

This simulation shows that the sediment distribution in Figure 1a is consistent with the description of Cenozoic sedimentation history developed from DSDP cores [*van Andel et al.*, 1975], though with a few amendments. Thin sediment north of the Clipperton fracture zone, which has been previously attributed to local current-induced erosion and enhanced carbonate dissolution with depth, is better described as part of a regional distortion of the equatorial sedimentary bulge caused by variable dissolution over a northwards deepening bathymetry gradient, the center of the bulge lying ~5° farther south than predicted without variable dissolution. This regional distortion results in thicker sediments at the present-day equator than would be expected without variable dissolution, as well as the thinning north of the Clipperton. Furthermore, the results suggest that this bathymetry gradient has persisted throughout much of the late Cenozoic. The gradient in basement topography probably reflects uplift of seafloor south of the equator caused by the Marquesas hotspot swell, thus implying a connection between mantle dynamics, which distort the Pacific seafloor, and the present shape of the equatorial sediment bulge. An overprediction in the model

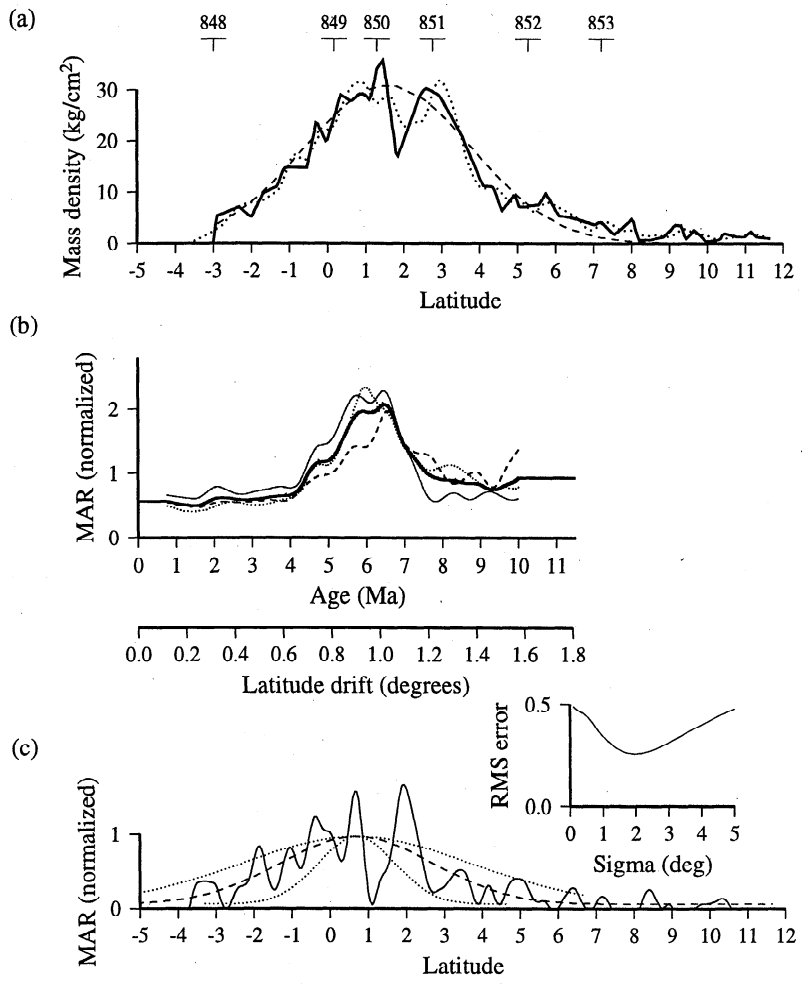

Figure A1. Deconvolution of a sediment mass distribution along a north-south profile at 110° W to correct for broadening caused by Pacific plate latitude drift. (a) Mass density profile (mass per unit seafloor area) from a seismic interpretation [*Mayer et al.*, 1992a]. Sediment thickness was computed from seismic two-way time using a second-order regression equation fitted to the sonic log data for ODP Sites 849, 850, and 851 [*Mayer et al.*, 1992b]. Mass density was then computed from the thicknesses using the regression equation given in the caption to Figure 4. The numbers above the profile show the ODP sites. The dashed line shows a Gaussian curve fitted to the data and the dotted line is a forward model of Figure A1b convolved with Figure A1c. (b) Bulk mass accumulation rate model used for $\mu(t)$. The three faint curves show MARs from Sites 849, 850, and 851 normalized to equal unit mean MAR (line convention as in Figure 12) and the bold line shows their average. The latitude drift corresponding to the age profile assumes a constant 0.1575°/m.y., computed from the rotations of *Duncan and Clague* [1985] for the center of the profile. (c) Result of inverting the mass density profile (Figure A1a) using the MAR model (Figure A1b) with an iterative algorithm [*Mitchell*, 1993, 1995b]. Irregularities are artefacts of the inversion so the center and width of the result are calculated by fitting the Gaussian curve (dashed line). The algorithm accuracy is indicated by the forward model (dotted line in Figure A1a). The inset shows the rms misfit error for the Gaussian curve in Figure A1c with variable width parameter σ. Gaussian curves with rms error 0.1 greater than the minimum are noticeably broader than the deconvolved curves, as illustrated by the two dotted curves constructed using 1° and 3° for σ. Hence the maximum error in σ is 1°.

immediately north of the Marquesas islands might reflect growth of the swell. This idea could be studied further with deep drilling by observing whether the CCD in older sediments north of the Marquesas swell is elevated compared to adjacent seafloor of similar latitude and age.

The results suggest reduced dissolution rates in the west of the area, and the modeled sediment distribution can be moderately improved by a CCD deepening by 10 m per degree of longitude. Although this gradient is not strongly resolved, it is comparable to that of the modern CCD [*Berger et al.*, 1976], suggesting that CCD gradients may have persisted throughout much of the Cenozoic. The breakdown of the model away from the central equatorial region may suggest other transitions in sediment supply, composition, or dissolution rates.

The comparison of the modeled and data center of mass for sediments on 30-45 Ma seafloor constrains the total Pacific plate drift since the Eocene to be 9.2°±3.6° of latitude (0-33.5 Ma according to the *Cande and Kent* [1995] timescale) and confirms the 39 Ma pole of *Sager and Pringle* [1988] to within 4°. The modeling favors a steady late Cenozoic motion for the Pacific plate relative to the equator, as previously suggested using drill core paleoequators [e.g., *van Andel et al.*, 1975]. Large abrupt

changes in latitude motion, such as predicted with some TPW models [*Andrews*, 1985; *Besse and Courtillot*, 1991], lead to anomalous sediment distributions in the simulations and generally support the view that the Pacific hotspots do not show evidence for TPW in the late Cenozoic. The paleolatitude uncertainty estimates are dominated by the extent to which sedimentation has coincided with the equator, and improvements in understanding the factors distorting equatorial sedimentation may later help to improve these error bounds. Accuracy also depends on the model's simple representation of mass accumulation rate variations with time, latitude and depth, and may need to be revised as further data become available from drilling.

The conclusions concerning TPW, however, assume a steady motion of the Pacific plate over the hotspots for 0-42 Ma [*Duncan and Clague*, 1985], while some have interpreted the curve in the Hawaiian chain and the oblique Marquesas chain as indicating an abrupt change in Pacific motion during the past few million years [*Wessel and Kroenke*, 1997]. Although this motion is poorly resolved, it is nevertheless potentially important because abrupt motion is not recorded in the sediment distribution or in the ODP Leg 138 sediments [*Pisias et al.*, 1995b]. Abrupt Pacific plate/hotspots motion would therefore require coincident TPW, possibly of ~200 km within the last few million years. Furthermore, these results do not generally preclude large TPW motion, which may be possible in the great circle plane perpendicular to the central Pacific. Discrepancies between different TPW models derived from paleomagnetic data and these sedimentary results suggest that more effort is required to resolve TPW before it can be reliably used to constrain geodynamic models of the motion.

Appendix: Inverse Model for the Latitude Distribution of Sediment Supply

The effect of northward Pacific motion on sediment stratigraphy illustrated in Figure 2 involves shifting of a function (isochrons) by varying amounts and summing to produce the net sediment load. This is analogous to a convolution process and suggests that it might be possible to recover the characteristic shape of the sedimentary isochrons by deconvolving the total sediment load obtained from seismic reflection records. This section develops and applies this model to a seismic section at 110°W in order to resolve the width of sedimentation for the forward modeling. The model is based on the assumption that sediment isochrons have not varied greatly in width or location. Although roughly justified by ODP data [*Pisias et al.*, 1995b], the results are only approximate due to errors in this assumption.

We assume that the latitude distribution of sedimentation has been constant, while the magnitude has fluctuated with time. The mass accumulation rate can then be expressed by $\mu(y)m(t)$, where $\mu(y)$ represents the distribution with latitude y and $m(t)$ represents the variation with time t before present. If we further assume that the Pacific plate has drifted northward with a constant velocity V, the total mass density at a point (M, kg/m^2) is

$$M(y_1,a) = \frac{1}{V}\int_{y_1-\Delta y}^{y_1} \mu(y)m\left(\frac{y_1-y}{V}\right)dy \qquad \text{(A1)}$$

where y_1 is the present latitude and Δy is the total latitude drift for seafloor of age a. Equation (A1) is a convolution equation in which the latitude drift of the plate via $m()$ effectively smears out the sediment latitude distribution $\mu()$, and therefore $\mu()$ might be recovered from measurements of the present sediment distribution $M(y_1, a)$ if $m(t)$ is known.

Sediment thickness interpreted from a north-south seismic line at 110°W [*Mayer et al.*, 1992a] was used to estimate $M(y_1, a)$. Seismic two-way times of *Mayer et al.* [1992a] were converted to sediment thickness using the sonic logs of ODP Sites 849, 850, and 851 [*Mayer et al.*, 1992b], which have been shown accurately to represent in situ velocity [*Bloomer et al.*, 1995]. These thicknesses were integrated with dry bulk densities from Sites 849, 850, and 851 using the regressions described in the caption to Figure 4. The result in Figure A1a shows a sediment bulge centered on 1.6°N with a 2σ width of 4.4° of latitude, estimated by fitting the dashed Gaussian curve. Because of errors due to interpreters typically picking the envelope of basement diffractions [*Mitchell*, 1995a], the coarse digitizing and irregularities of the profile (artefacts of sediment redistribution), the following aims to determine only the center and width of sedimentation, not the finer details. (If further seismic lines become available, combining several profiles may improve the results, although studying the seismic stratigraphy [*Bloomer et al.*, 1995] may also reveal these details without the need for the assumption of constant latitude distribution of sedimentation.)

The fluctuations in MAR with time $\mu(t)$ were determined from ODP core data. Figure 12 shows the results of combining a revised stratigraphy [*Shackleton et al.*, 1995] with dry bulk densities for the 110°W sites [*Mayer et al.*, 1992b]. To produce a model for $\mu(t)$, the three deepest holes (849, 850, and 851) were normalized to equal MAR and averaged (solid curve in Figure A1b). The model was extrapolated to 11.5 Ma, which is the average basement age for the 110°W transect based on oldest sediment or extrapolation for wells shallower than basement. These core dates and seafloor magnetic anomaly trends suggest only minor variations in basement age across the center of the profile. The second ordinate in Figure A1b shows the latitude drift for 110°W according to the Pacific hotspot model of *Duncan and Clague* [1985].

Figure A1c shows the result of deconvolving the mass density profile in Figure A1a using Figure A1b (the irregularity is an artefact of the inversion enlarging irregularities in Figure A1a). The simple iterative algorithm described by *Mitchell* [1993, 1995b] was used since it allows the result to be constrained to be positive. The Gaussian dashed curve fitted to Figure A1c indicates that 0-11.5 Ma deposition has been centered on 0.7°N with a 2σ width of 4.0°.

Acknowledgments. This study is based on a digital sediment isopach map from the National Geophysical Data Center [*Divins and Eakins*, 1997], a digital seafloor age map [*Muller et al.*, 1997] and seismic data from Scripps Institution of Oceanography collected on the Crossgrain-1 cruise led by E. L. Winterer. The figures were created with the GMT software [*Wessel and Smith*, 1991]. I am grateful to R. A. Livermore and S. Bloomer for discussions on true polar wander and Pacific sedimentation. I thank E. L. Winterer, G. D. Acton, and P. Wessel for critical reviews which significantly improved this manuscript. This work was supported by Natural Environment Research Council Fellowship GT5/92/GS/5 and by a Royal Society University Research Fellowship.

References

Acton, G. D., and R. G. Gordon, Paleomagnetic tests of Pacific plate reconstructions and implications for motion between hotspots, *Science, 263*, 1246-1254, 1994.

Andrews, J. A., True polar wander: An analysis of Cenozoic and Mesozoic paleomagnetic poles, *J. Geophys. Res., 90*, 7737-7750, 1985.

Arrhenius, G., Sediment cores from the East Pacific, *Rep. Swed. Deep Sea Exped. (1947-1948), Parts 1-4, 5,* 1-288, 1952.

Barron, J. A., C. A. Nigrini, A. Pujos, T. Saito, F. Theyer, E. Thomas, and N. Weinreich, Synthesis of biostratigraphy, central equatorial Pacific, Deep Sea Drilling Project Leg 85: Refinement of Oligocene to Quaternary biochronology, in *Initial Rep. Deep Sea Drill. Proj., 85,* 905-934, 1985.

Berger, W. H., Cenozoic sedimentation in the eastern tropical Pacific, *Geol. Soc. Am. Bull., 84,* 1941-1954, 1973.

Berger, W. H., Sedimentation of deep-sea carbonate: Maps and models of variations and fluctuations, *J. Foraminiferal Res., 8,* 286-302, 1978.

Berger, W. H., and E. L. Winterer, Plate stratigraphy and the fluctuating carbonate line, *Spec. Pub. Int. Assoc. Sedimentol., 1,* 11-48, 1974.

Berger, W. H., C. G. Adelseck, and L. A. Mayer, Distribution of carbonate in surface sediments of the Pacific Ocean, *J. Geophys. Res., 81,* 2617-2627, 1976.

Berger, W. H., M.-C. Bonneau, and F. L. Parker, Foraminifera on the deep-sea floor: Lysocline and dissolution rate, *Oceanol. Acta, 5,* 249-258, 1982.

Besse, J., and V. Courtillot, Revised and synthetic apparent polar wander paths of the African, Eurasian, North-American and Indian plates, and true polar wander since 200 Ma, *J. Geophys. Res., 96,* 4029-4050, 1991.

Bloomer, S. F., L. A. Mayer, and T. C. Moore, Seismic stratigraphy of the eastern equatorial Pacific Ocean: Paleoceanographic implications, *Proc. Ocean Drill. Program Sci. Results, 138,* 537-553, 1995.

Boyce, R. E., Leg 75 methods for laboratory-measured physical properties, Gearhart-Owen well logs, and the Uyeda downhole temperature probe, *Initial Rep. Deep Sea Drill. Proj., 75,* 1179-1187, 1982.

Cande, S. C., and D. V. Kent, Revised calibration of the geomagnetic polarity timescale for the late Cretaceous and Cenozoic, *J. Geophys. Res., 100,* 6093-6095, 1995.

Christensen, U., Fixed hotspots gone with the wind, *Nature, 391,* 739-740, 1998.

Clague, D. A., and R. D. Jarrard, Tertiary Pacific plate motion deduced from the Hawaiian-Emperor chain, *Geol. Soc. Am. Bull., 84,* 1135-1154, 1973.

Cox, A., and D. Engebretson, Change in motion of Pacific plate at 5 Myr BP, *Nature, 313,* 472-474, 1985.

Divins, D. L., and B. Eakins, Total sediment thickness map for the southeast Pacific Ocean, in *International Geological-Geophysical Atlas of the Pacific Ocean*, in press, edited by G. B. Udintsev, Intergovernmental Oceanogr. Comm., 1997.

Duncan, R. A., and D. Clague, Pacific plate motion is recorded by linear volcanic chains, in *The Ocean Basins and Margins,* Vol. 7A, edited by A. E. M. Nairn, F. G. Stehli, and U. Uyeda, pp. 89-121, Plenum, New York, 1985.

Eittreim, S. L., N. Ragozin, H. S. Gnibidenko, and C. E. Helsley, Crustal age between the Clipperton and Clarion fracture zones, *Geophys. Res. Lett., 19,* 2365-2368, 1992.

Engebretson, D. C., Relative motions between oceanic and continental plates in the Pacific basin, *Spec. Pap. Geol. Soc. Am., 206,* 1-59, 1985.

Farrell, F. J., and W. L. Prell, Climatic change and $CaCO^3$ preservation: An 800,000 year bathymetric reconstruction from the central equatorial Pacific Ocean, *Paleoceanography, 4,* 447-466, 1989.

Farrell, J. W., and W. L. Prell, Pacific $CaCO_3$ preservation and $\delta^{18}O$ since 4 Ma: Paleoceanographic and paleoclimatic implications, *Paleoceanography, 6,* 485-498, 1991.

Farrell, J. W., I. Raffi, T. R. Janecek, D. W. Murray, M. Levitan, K. Dadey, K.-C. Emeis, M. Lyle, J.-A. Flores, and S. Hovan, Late Neogene sedimentation patterns in the eastern equatorial Pacific Ocean, *Proc. Ocean Drill. Program Sci. Results, 138,* 717-756, 1995.

Goff, J. A., and J. R. Cochran, The Bauer scarp jump: A complex tectonic sequence revealed in satellite altimetry, *Earth Planet. Sci. Lett., 141,* 21-33, 1996.

Goldreich, P., and A. Toomre, Some remarks on polar wandering, *J. Geophys. Res., 74,* 2555-2567, 1969.

Gordon, R. G., and C. D. Cape, Cenozoic latitudinal shift of the Hawaiian hotspot and its implications for true polar wander, *Earth Planet. Sci. Lett., 55,* 37-47, 1981.

Hamilton, E. L., Variations of density and porosity with depth in deep-sea sediments, *J. Sediment. Petrol. 46,* 280-300, 1976.

Harrison, C. G. A., and T. Lindh, A polar wandering curve for North America during the Mesozoic and Cenozoic, *J. Geophys. Res., 87,* 1903-1920, 1982.

Heath, G. R., and C. Culberson, Calcite: Degree of saturation, rate of dissolution and the compensation depth in the deep ocean, *Geol. Soc. Am. Bull, 81,* 3157-3160, 1970.

Heath, G. R., T. C. Moore, and T. H. van Andel, Carbonate accumulation and dissolution in the equatorial Pacific during the past 45 million years, in *The Fate of Fossil Fuel CO_2 in the Oceans*, *Mar. Sci. Ser.* vol. 6, edited by N. R. Andersen and A. Malahoff, pp. 627-639, Plenum, New York, 1977.

Herron, E. M., Sea-floor spreading and the Cenozoic history of the east-central Pacific, *Geol. Soc. Am. Bull., 83,* 1671-1692, 1972.

Houtz, R. E., and W. J. Ludwig, Distribution of reverberant subbottom layers in the southwest Pacific basin, *J. Geophys. Res., 84,* 3497-3504, 1979.

Johnson, D. A., Eastward flowing bottom currents along the Clipperton Fracture Zone, *Deep Sea Res., 19,* 253-257, 1972a.

Johnson, D. A., Ocean-floor erosion in the equatorial Pacific, *Geol. Soc. Am. Bull., 83,* 3121-3144, 1972b.

Kane, K. A., and D. E. Hayes, A new relationship between subsidence rate and zero-age depth, *J. Geophys. Res., 99,* 21759-21777, 1994.

Lancelot, Y., Relations entre evolution sedimentaire et tectonique de la plaque Pacifique depuis le Cretace inferieur, *Mem. Hors-Ser. Soc. Geol. Fr., 134,* 1-40, 1978.

Larson, K. M., J. T. Freymueller, and S. Philipsen, Global plate velocities from the Global Positioning System, *J. Geophys. Res., 102,* 9961-9981, 1997.

Leinen, M., Biogenic silica accumulation in the central equatorial Pacific and its implications for Cenozoic paleoceanography: Summary, *Geol. Soc. Am. Bull., 90,* 801-803, 1979.

Livermore, R. A., F. J. Vine, and A. G. Smith, Plate motions and the geomagnetic field, I, Quaternary and late Tertiary, *Geophys. J. R. Astron. Soc., 73,* 153-171, 1983.

Ludwig, W. J., and R. E. Houtz, Isopach map of the sediments in the Pacific Ocean Basin, color map with text, Am. Assoc. of Pet. Geol., Tulsa, Okla., 1979.

Lyle, M., Composition maps of surface sediments of the eastern tropical Pacific Ocean, *Ocean Drill. Program Initial Rep., 138,* 101-115, 1992.

Mayer, L., and F. Theyer, Initial Reports Deep Sea Drilling Project, vol. 85, U.S. Govt. Print. Off., Washington, D.C., 1985.

Mayer, L. A., et al., Introduction, *Proc. Ocean Drill. Program Initial Rep., 138,* 5-12, 1992a.

Mayer, L. A., et al., *Proceedings of the Ocean Drilling Program, Initial Reports*, vol 138, Ocean Drill. Program, College Station, Tex., 1992b.

McNutt, M. K., and K. M. Fisher, The South Pacific Superswell, in *Seamounts, Islands, and Atolls, Geophys. Monogr. Ser.*, vol. 43, edited by B. H. Keating et al., pp. 25-34, AGU, Washington, D. C., 1987.

Mitchell, N. C., A model for attenuation of backscatter due to sediment accumulations and its application to determine sediment thickness with GLORIA sidescan sonar, *J. Geophys. Res., 98,* 22477-22493, 1993.

Mitchell, N. C., Characterising the extent of volcanism at the Galapagos Spreading Centre using Deep Tow profiler records, *Earth Planet. Sci. Lett., 134,* 459-472, 1995a.

Mitchell, N. C., Representing backscatter fluctuations with a PDF convolution equation, and its application to study backscatter variability in side-scan sonar images, *IEEE Trans. Geosci. Remote Sens., 33,* 1328-1331, 1995b.

Molnar, P., and J. Stock, Relative motions of hotspots in the Pacific, Atlantic and Indian Oceans since late Cretaceous time, *Nature, 327,* 587-591, 1987.

Moore, T. C., G. R. Heath, and R. O. Kowsmann, Biogenic sediments of the Panama Basin, *J. Geol., 81,* 458-472, 1973.

Muller, R. D., W. R. Roest, J.-Y. Roger, L. M. Gahagan, and J. G. Sclater, Digital isochrons of the world's ocean floor, *J. Geophys. Res., 102,* 3211-3214, 1997.

Parsons, B., and J. G. Sclater, An analysis of the variation of ocean floor bathymetry and heat flow with age, *J. Geophys. Res., 82,* 803-827, 1977.

Pena, M. A., M. R. Lewis, and W. G. Harrison, Primary productivity and size structure of phytoplankton biomass on a transect of the equator at 135°W in the Pacific Ocean, *Deep Sea Res., 37,* 295-315, 1990.

Petronotis, K. E., R. G. Gordon, and G. D. Acton, A 57 Ma Pacific plate palaeomagnetic pole determined from a skewness analysis of crossings of marine magnetic anomaly 25r, *Geophys. J. Int., 118,* 529-554, 1994.

Pisias, N. G., L. A. Mayer, T. R. Janecek, A. Palmer-Julson, and T. H. van Andel, *Proceedings of the Ocean Drilling Program, Scientific Results, 138*, Ocean Drill. Program, College Station, Tex., 1995a.

Pisias, N. G., L. A. Mayer, and A. C. Mix, Paleoceanography of the eastern equatorial Pacific during the Neogene: Synthesis of Leg 138 drilling results, in *Proc. Ocean Drill. Program,Sci. Results, 138*, 5-21, 1995b.

Rea, D. K., and M. Leinen, Neogene history of the calcite compensation depth and lysocline in the South Pacific Ocean, *Nature, 316,* 805-807, 1985.

Richards, M. A., Y. Ricard, C. Lithgow-Bertelloni, G. Spada, and R. Sabadini, An explanation for Earth's long-term rotational stability, *Science, 275,* 372-375, 1997.

Sager, W. W., Paleomagnetism of Abbott Seamount and implications for the latitudinal drift of the Hawaiian hot spot, *J. Geophys. Res., 89,* 6271-6284, 1984.

Sager, W. W., and M. S. Pringle, Mid-Cretaceous to Early Tertiary apparent polar wander path of the Pacific plate, *J. Geophys. Res., 93,* 11753-11771, 1988.

Sandwell, D. T., and W. H. F. Smith, Marine gravity anomaly from Geosat and ERS-1 satellite altimetry, *J. Geophys. Res., 102,* 10039-10054, 1997.

Shackleton, N. J., S. Crowhurst, T. Hagelberg, N. G. Pisias, and D. A. Schneider, A new late Neogene time scale: Application to Leg 138 sites, *Proc. Ocean Drill. Program, Sci. Results, 138*, 1995.

Shipley, T. H., E. L. Winterer, M. Goud, S. J. Mills, C. V. Metzler, C. K. Paull, and J. T. Shay, Seabeam bathymetric and water-gun seismic reflection surveys in the equatorial Pacific, *Initial Rep. Deep Sea Drill. Proj., 85,* pp. 825-837, 1985.

Smith, W. H. F., and P. Wessel, Gridding with continuous curvature splines in tension, *Geophysics, 55,* 293-305, 1990.

Stein, C. A., and S. Stein, Constraints on Pacific midplate swells from global depth-age and heat flow-age models, in *The Mezocoic Pacific: Geology, Tectonics, and Volcanism*, *Geophys. Monogr. Ser.*, vol. 77, edited by M. S. Pringle et al., pp. 53-76, AGU, Washington, D. C., 1993.

Steinberger, B., and R. J. O'Connell, Changes of the Earth's rotation axis owing to advection of mantle density heterogeneities, *Nature, 387,* 169-173, 1997.

Suarez, G., and P. Molnar, Paleomagnetic data and pelagic sediment facies and the motion of the Pacific plate relative to the spin axis since the Late Cretaceous, *J. Geophys. Res., 85,* 5257-5280, 1980.

Theyer, F., L. A. Mayer, and E. Thomas, The equatorial Pacific high-productivity belt: Elements for a synthesis of Deep Sea Drilling Project Leg 85 results, *Initial Rep. Deep Sea Drill. Proj., 85,* 971-985, 1985.

Tracey, J. I., *Initial Reports Deep Sea Drilling Project,* vol. 8, U.S. Govt. Print. Off., Washington, D. C., 1971.

van Andel, T. H., and D. Bukry, Basement ages and basement depths in the eastern equatorial Pacific, *Geol. Soc. Am. Bull., 84,* 2361-2370, 1973.

van Andel, T. J., G. R. Heath, and T. C. Moore, Cenozoic tectonics, sedimentation, and paleoceanography of the central equatorial Pacific, *Mem. Geol. Soc. Am., 143,* 1-134, 1975.

Wessel, P., and L. Kroenke, A geometric technique for relocating hotspots and refining absolute plate motions, *Nature, 387,* 365-369, 1997.

Wessel, P., and W. H. F. Smith, Free software helps map and display data, *Eos Trans. AGU, 72,* 441, 1991.

Wilkens, R. H., and T. Handyside, Physical properties of equatorial Pacific sediments, *Initial Rep. Deep Sea Drill. Proj., 85,* 1985.

Winterer, E. L., Sedimentary facies and plate teconics of the Equatorial Pacific, *Am. Assoc. Pet. Geol. Bull., 57,* 265-282, 1973.

Winterer, E. L., Anomalies in the tectonic evolution of the Pacific, in *The Geophysics of the Pacific Ocean Basin and Its Margin, A Volume in Honor of George P. Woollard, Geophys. Monogr. Ser.*, vol. 19, edited by G. H. Sutton, M. H. Manghnani, and R. Moberly, pp. 269-278, AGU, Washington, D. C., 1976.

Winterer, E. L., and D. T. Sandwell, Evidence from en-echelon cross-grain ridges for tensional cracks in the Pacific plate, *Nature, 329,* 534-537, 1987.

Worsley, T. R., and T. A. Davies, Cenozoic sedimentation in the Pacific Ocean: Steps toward a quantitative evaluation, *J. Sediment. Petrol., 49,* 1131-1146, 1979.

N. C. Mitchell, Department of Earth Sciences, University of Oxford, Parks Road, Oxford OX1 3PR, England. (e-mail: neilm@earth.ox.ac.uk)

(Received September 2, 1997; revised March 13, 1998; accepted May 7, 1998.)